

CapZ regulates autophagosomal membrane shaping by promoting actin assembly inside the isolation membrane

Na Mi^{1,5,6}, Yang Chen^{1,5}, Shuai Wang², Mengran Chen², Mingkun Zhao¹, Guang Yang¹, Meisheng Ma¹, Qian Su³, Sai Luo¹, Jingwen Shi¹, Jia Xu¹, Qiang Guo⁴, Ning Gao⁴, Yujie Sun³, Zhucheng Chen^{2,6} and Li Yu^{1,6}

A fundamental question regarding autophagosome formation is how the shape of the double-membrane autophagosomal vesicle is generated. Here we show that in mammalian cells assembly of an actin scaffold inside the isolation membrane (the autophagosomal precursor) is essential for autophagosomal membrane shaping. Actin filaments are depolymerized shortly after starvation and actin is assembled into a network within the isolation membrane. When formation of actin puncta is disrupted by an actin polymerization inhibitor or by knocking down the actin-capping protein CapZ β , isolation membranes and omegasomes collapse into mixed-membrane bundles. Formation of actin puncta is PtdIns(3)P dependent, and inhibition of PtdIns(3)P formation by treating cells with the PI(3)K inhibitor 3-MA, or by knocking down Beclin-1, abolishes the formation of actin puncta. Binding of CapZ to PtdIns(3)P, which is enriched in omegasomes, stimulates actin polymerization. Our findings illuminate the mechanism underlying autophagosomal membrane shaping and provide key insights into how autophagosomes are formed.

Autophagy is an evolutionarily conserved degradation pathway^{1–3}. Autophagosome formation is a very complicated cellular process⁴. In mammalian cells, autophagosomes are formed on PtdIns(3)P-enriched endoplasmic reticulum (ER) protrusions named omegasomes, which appear shortly after starvation^{5–7}. Omegasomes give rise to intermediate structures named isolation membranes (phagophores)⁸, which start as small, relatively flat cisternae and grow into curved, cup-shaped double-membrane structures⁹. At this stage, the isolation membrane seems to be a dome-shaped cisterna with an open base, which is connected to a PtdIns(3)P-enriched omegasome. The opening is finally sealed to give rise to the double-membrane vesicle. Once formed, the autophagosome exits from the ER and the omegasome is retracted back into the ER (ref. 5).

One of the fundamental questions regarding autophagosome formation is how membrane shape is generated and maintained during expansion of the isolation membrane. The process by which autophagosomes are formed is unique among intracellular vesicles. Most intracellular vesicles, for example, endocytic vesicles or transport vesicles, are generated through a budding process¹⁰. The autophagosome, in contrast, is formed by expansion and bending

of membrane cisternae¹¹; thus, there must be a shaping mechanism to generate and maintain the unique cup shape of the isolation membrane during autophagosome formation.

Actin bundles or branched actin arrays can cause membrane deformation by generating a propulsion force and by forming internal scaffolding^{12,13}. The best example of actin-induced membrane deformation is lamellipodia formation¹². During lamellipodia formation, the actin network on the leading edge of the cell creates a propulsion force that deforms the plasma membrane to form membrane protrusions¹⁴. The roles of the actin cytoskeleton in autophagy are complicated; in mammalian cells, actin is required for autophagy and participates in different steps of autophagosome formation^{15,16}. ATG14 and Beclin1, but not Atg5 or LC3, have been shown to co-localize with actin during autophagy¹⁵.

RESULTS

Formation of actin puncta during autophagy

In normal rat kidney (NRK) cells, serum/glutamine starvation induces autophagy that peaks at 4 h after starvation¹⁷ (Supplementary Fig. 1a and Supplementary Video 1). We found that actin undergoes dynamic

¹The State Key Laboratory of Membrane Biology, Tsinghua University-Peking University Joint Center for Life Sciences, School of Life Sciences, Tsinghua University, Beijing 100084, China. ²Center for Structural Biology, Tsinghua University, Beijing 100084, China. ³The State Key Laboratory of Membrane Biology, Biodynamic Optical Imaging Center, School of Life Sciences, Peking University, Beijing 100871, China. ⁴Ministry of Education Key Laboratory of Protein Sciences, Center for Structural Biology, School of Life Sciences, Tsinghua University, Beijing 100084, China. ⁵These authors contributed equally to this work.

⁶Correspondence should be addressed to N.M., Z.C. or L.Y. (e-mail: mina@mail.tsinghua.edu.cn or zhucheng_chen@mail.tsinghua.edu.cn or liyulab@mail.tsinghua.edu.cn)

Received 30 August 2014; accepted 1 July 2015; published online 3 August 2015; DOI: 10.1038/ncb3215

depolymerization shortly after starvation. Using phalloidin, a probe for polymerized actin¹⁸, we found that NRK cells growing in nutrient-rich conditions contained many actin filaments (Fig. 1a). At 2 h after starvation, phalloidin-positive puncta started to appear in starved cells, suggesting that a polymerized actin structure was forming (Fig. 1a). Co-staining starved cells with anti-LC3 antibody and phalloidin showed that many of these actin puncta co-localized with the autophagosome marker LC3 (Fig. 1b and Supplementary Fig. 1b)¹⁹. Quantification of the number of LC3 puncta co-localizing with phalloidin indicated that a significant proportion of LC3-positive puncta contained actin (Fig. 1c). In non-starved cells, a few small LC3 puncta and actin puncta were also observed; however, they did not co-localize (Fig. 1d). To further validate this observation, we established a cell line expressing GFP-LC3 and Lifeact-mRFPuby, a widely used probe for polymerized actin²⁰. Live-cell imaging showed that Lifeact formed puncta inside LC3 puncta (Fig. 1e).

Actin puncta are co-localized with isolation membranes

LC3 puncta can be autophagosomes or isolation membranes; therefore, to determine the exact nature of these phalloidin-positive puncta, we quantified co-localization of phalloidin with puncta positive for DFCP1 (a PtdIns(3)P-binding ER protein that marks omegasomes^{21–23}) and LC3, as isolation membranes are both DFCP1- and LC3-positive whereas mature autophagosomes are DFCP1-negative. Most phalloidin-positive structures were LC3/DFCP1-positive (Fig. 2a,b), indicating that isolation membranes are the main site of actin assembly. We also showed that phalloidin co-localized with other proteins localized on isolation membranes, including Atg5, ULK1, Atg14 and Atg16 (Fig. 2c).

Actin networks localize inside the central cavity of isolation membranes/autophagosomes

Next, we investigated the spatial relationship between LC3 puncta and actin puncta. We found that the actin puncta seemed in many cases to be localized within the boundary of LC3 puncta (Fig. 1b,e). To better illustrate the location of the actin puncta, we used structured illumination microscopy (SIM)²⁴, which allows us to acquire super-resolution three-dimensional (3D) or 2D images. SIM images of actin and LC3 confirm that actin puncta were localized inside the isolation membranes (Fig. 3a,b). From these data, we conclude that actin puncta are assembled inside the isolation membrane. Next, we permeabilized cells with digitonin to prepare semi-intact cells, in which soluble cytosol was removed while membrane structures are largely intact. SIM images showed that the phalloidin signal is markedly reduced in semi-intact cells, with no visible actin filaments left, indicating that cytosolic actin was removed (Fig. 3c). Interestingly, most of the remaining phalloidin signal was enriched on plasma membranes and inside LC3 puncta. In some cases, phalloidin formed ring-like structures that closely associated with LC3 puncta (Fig. 3c), indicating that polymerized actin closely associated with the inner membrane of isolation membranes. Furthermore, immuno-electron microscopy analysis of actin-GFP-expressing cells confirmed that the actin is localized inside isolation membranes (Fig. 3d–f). Treating cells with bafilomycin A1 (BAF-A1), which blocks the fusion between mature autophagosomes and lysosomes²⁵, caused massive accumulation of

actin puncta in autophagosomes (Fig. 3g), further confirming that actin is present in mature autophagosomes.

Actin puncta contain branched actin networks

Cofilin is an actin-dynamizing protein, which can bind and sever actin filaments^{26–30}. We found that the localization of cofilin changed markedly during autophagy. Cofilin has a diffuse, cytosolic localization pattern in cells grown in nutrient-rich conditions. However, 4 h after starvation, cofilin forms puncta (Fig. 4a), and a significant percentage of these puncta are inside LC3 puncta (Fig. 4b). The presence of cofilin in isolation membranes indicates that the actin puncta may contain branched actin networks, as it is known that cofilin can be enriched on branched actin networks^{31,32}. It is well established that branched actin networks can cause membrane deformation by generating a propulsion force and by forming internal scaffolding³³. Formation of branched actin networks requires activation of the branched actin nucleator complex Arp2/3, which binds to actin filaments and forms the first subunit of a new branch^{34–38}. To test whether the actin puncta inside isolation membranes are branched actin networks, we transfected cells with ARPC1B (also known as p41-Arc), a subunit of the Arp2/3 complex³⁸. We found that ARPC1B forms puncta after starvation, and these puncta are co-localized with LC3 in a manner very similar to the co-localization pattern between cofilin and LC3 (Fig. 4c,d). These data suggest that the actin puncta do indeed contain branched actin networks.

CapZ regulates autophagy

Actin polymerization is spatially and temporally regulated by various factors to ensure the proper assembly of membrane protrusions^{39–41}. The actin-capping protein CapZ has been shown to bind actin and to be required for formation of membrane protrusions, and plasma membrane-enriched phosphoinositides, especially PtdIns(4,5)P₂, play important roles in spatial and temporal regulation of the formation of membrane protrusions^{42–44}. We studied the role of CapZ in autophagosome formation. First, we measured the degradation of long-lived proteins, a standard assay for autophagy activity, and found that *Capzb* knockdown caused impaired degradation of long-lived proteins in NRK cells starved in DPBS starvation buffer, which is a stronger inducer of autophagy compared with the serum/glutamine starvation we used in imaging analysis⁴⁵ (Fig. 5a and Supplementary Fig. 2a). Similarly, treatment with the actin polymerization inhibitor cytochalasin B or CK636, a compound that inhibits the formation of branched actin networks³⁴, potently inhibited the degradation of long-lived proteins (Fig. 5b). Degradation of the autophagy substrate p62 (Fig. 5c,d) was similarly impaired in *Capzb* knockdown cells, indicating that autophagy is impaired when *Capzb* function is reduced⁴⁶. LC3-II processing is apparently normal in *Capzb* knockdown cells (Supplementary Fig. 2a,b), suggesting that autophagy is impaired at a step after LC3 processing. The number of autophagosomes is not altered in *Capzb* knockdown cells; however, the morphology of LC3 puncta was markedly altered. In nonspecific-RNAi-transfected cells, most LC3 puncta were round; in contrast, many *Capzb* knockdown cells contained tubular or enlarged ring-shaped LC3 puncta (Fig. 5e,f and Supplementary Fig. 2c–e). A similar phenotype was observed in *Capzb* knockdown

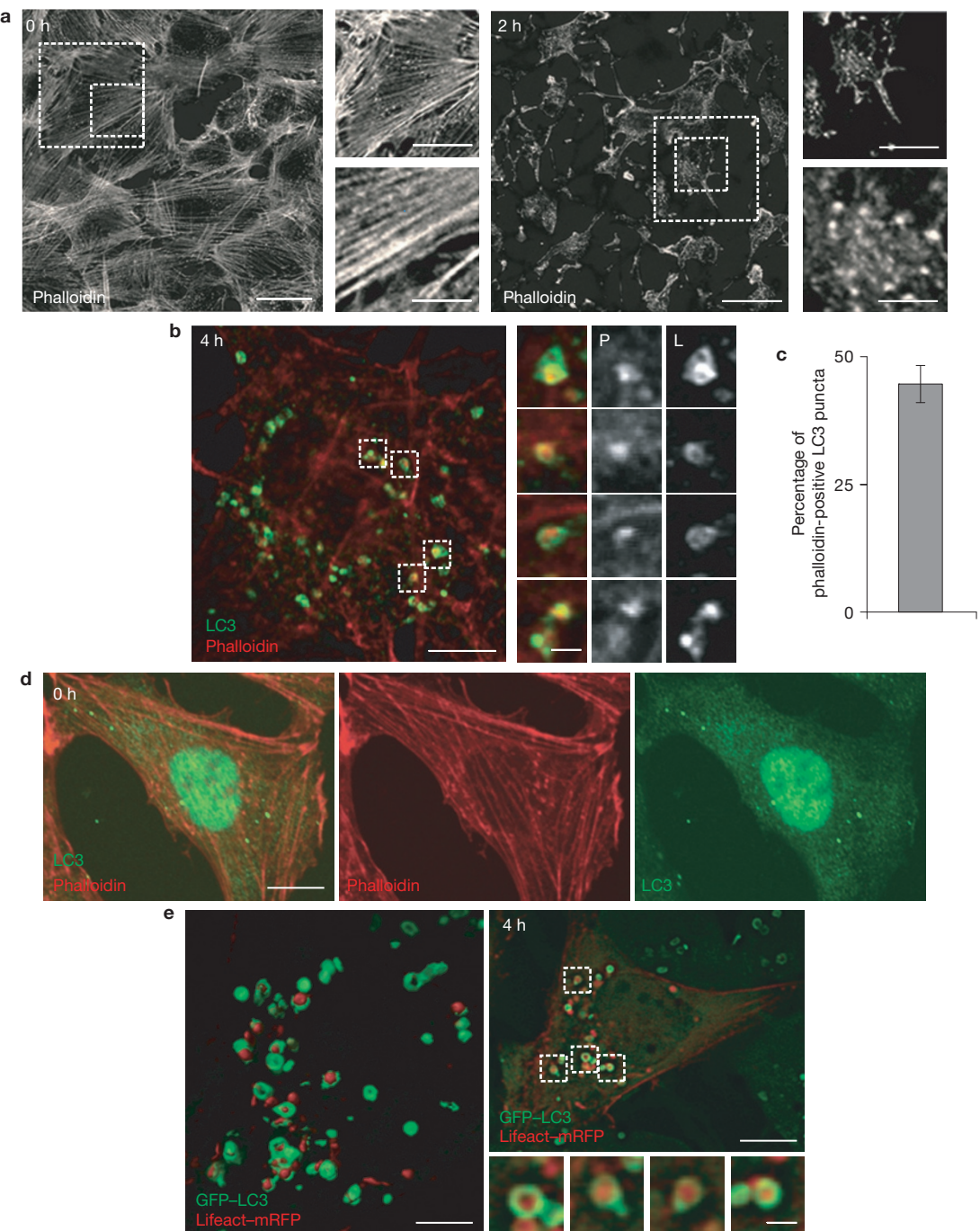


Figure 1 Formation of actin puncta during autophagy. (a) Representative image of NRK cells starved for 0 or 2 h and stained with phalloidin. Regions outlined with white dashed lines are magnified to the right. Scale bars in full panels and zoomed panels correspond to 20 μ m, 15 μ m and 8 μ m, respectively. (b) NRK cells were starved for 4 h then stained with phalloidin (P) and antibody against LC3 (L). Regions of LC3 puncta that co-localize with phalloidin are outlined with white dashed lines and are magnified to the right. Scale bars in full panels and zoomed panels correspond to 5 μ m and 1 μ m, respectively. (c) The percentage of phalloidin-positive LC3 puncta

was quantified in cells from b ($n=3$ independent experiments; 50 cells were assessed per independent experiment). Data represent mean \pm s.d. (d) NRK cells were stained with LC3 antibody and phalloidin. Scale bar, 5 μ m. (e) GFP-LC3-expressing NRK cells were transfected with Lifeact-mRFP, and then starved for 4 h. Left panel shows the 3D-reconstruction image; right panel shows a single plane from a single stack from the cell in the left panel. Regions showing Lifeact-positive dots inside LC3-positive rings are outlined with white dashed lines and are magnified below. Scale bars in full panels and zoomed panels correspond to 5 μ m and 1 μ m, respectively.

Raw cells (Supplementary Fig. 2f,g). This phenotype can be rescued by overexpression of an RNAi-resistant *Capzb* plasmid in *Capzb* knockdown cells (Supplementary Fig. 2h–j). To check whether

Capzb knockdown affects omegasome formation, we established an NRK cell line expressing a GFP fusion of the omegasome marker protein DFCP1 (ref. 5). We found that *Capzb* knockdown

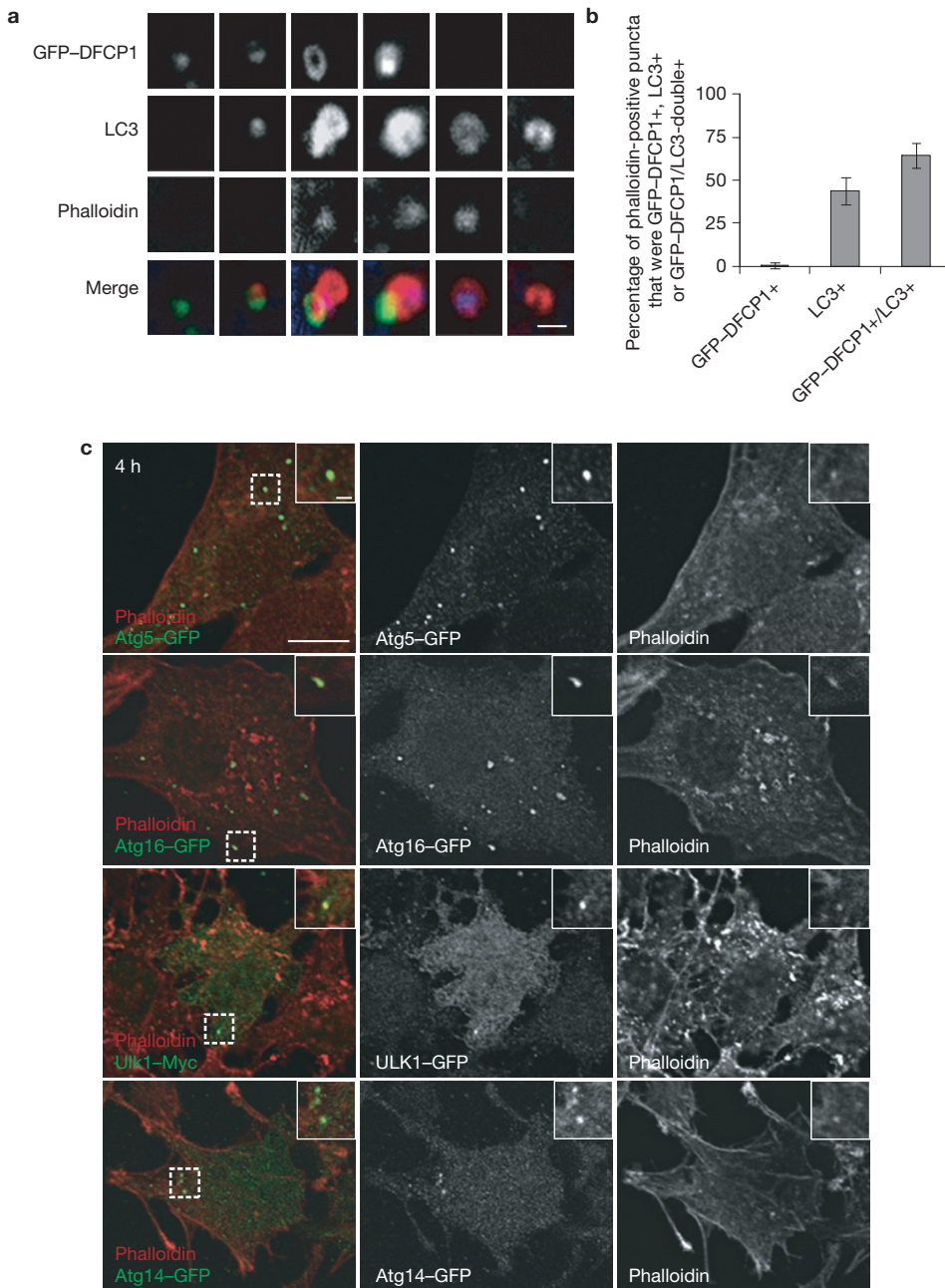


Figure 2 Actin puncta are co-localized with isolation membranes. **(a)** Representative images of GFP-DFCP1-positive, GFP-DFCP1/LC3-double-positive and LC3-positive puncta in a pool of phalloidin-positive puncta in stable GFP-DFCP1-expressing NRK cells. The cells were stained with phalloidin and antibodies against LC3 and GFP. Scale bar, 1 μm. **(b)** Cells from **a** were quantified for phalloidin-positive structures that were GFP-DFCP1-positive, LC3-positive or GFP-DFCP1/LC3-double-

positive ($n=3$ independent experiments; 50 cells were assessed per independent experiment). Data represent mean \pm s.d. **(c)** NRK cells expressing Atg5-GFP, Atg16-GFP, ULK1-Myc or Atg14-GFP were starved for 4 h and stained with phalloidin and anti-GFP/anti-Myc antibody. Regions outlined with white dashed lines are magnified in the insets. Scale bars in full panels and zoomed panels correspond to 5 μm and 1 μm, respectively.

caused formation of enlarged omegasomes with ring-shaped or short tubular morphology (Supplementary Fig. 3a). In normal cells, autophagosomes emerge from DFCP1-positive omegasomes, and the DFCP1 signal then disappears as the omegasomes are retracted back into the ER. In *Capzb* knockdown cells, the LC3 and DFCP1 puncta had abnormal morphology and the co-localization of LC3 with DFCP1 was increased (Fig. 5e–h), implying that autophagosome

formation is impaired. It is worth noting that DFCP1 and LC3 do not show any obvious abnormality when *Capzb* knockdown cells are grown in nutrient-rich conditions (Supplementary Fig. 3b). In cells that were briefly treated with the specific Arp2/3 inhibitor CK666 at 1 h after starvation, tubular or enlarged ring-shaped LC3 puncta and enhanced DFCP1/LC3 co-localization were observed (Supplementary Fig. 4a–d), as in *Capzb* knockdown cells.

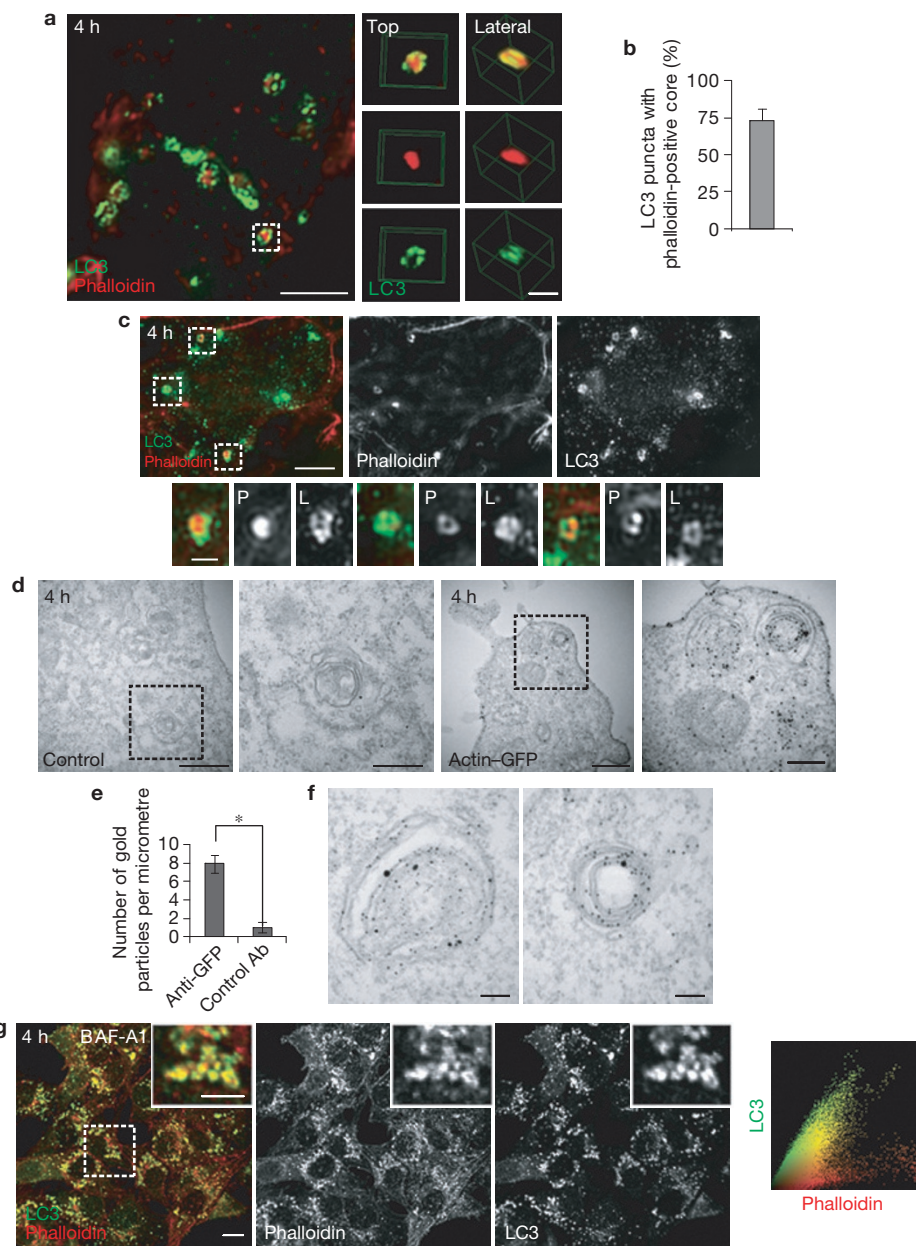


Figure 3 Actin puncta localize inside the central cavity of isolation membranes/autophagosomes. (a) NRK cells were starved for 4 h, then stained with phalloidin and antibodies against LC3 and observed by 3D-SIM. The left panels show a single plane from a single stack from one cell. Right panels show enlarged 3D reconstructions of LC3-positive structures outlined with white dashed lines in the left panel. Scale bars in full panels and zoomed panels correspond to 5 μm and 1 μm. (b) Cells from a were quantified for LC3-positive puncta with a phalloidin-positive core ($n=3$ independent experiments; 50 cells were assessed per independent experiment). Data represent mean \pm s.d. (c) NRK cells were starved for 4 h. Semi-intact cells were prepared and then stained with phalloidin (P) and anti-LC3 antibody (L). Regions of interest are outlined with white dashed lines and magnified below. Scale bars in full panels and zoomed panels correspond to 5 μm and 1 μm, respectively. (d) Actin-GFP-expressing NRK cells were

starved for 4 h and then analysed by immuno-electron microscopy using antibodies against GFP. Regions of interest are outlined with white dashed lines and magnified to the right. Scale bars in full panels and zoomed panels correspond to 500 nm and 200 nm, respectively. (e) The number of nanogold particles per micrometre on autophagosome membranes from d was quantified ($n=3$ independent experiments; 30 fields were assessed per independent experiment). Data represent mean \pm s.d. * $P<0.05$ (two-tailed t-test). (f) Representative images of isolation membranes in cells from d. Scale bars, 100 nm. (g) NRK cells were starved for 4 h with or without 100 nM BAF-A1 and then observed by confocal microscopy. Regions of interest are outlined with white dashed lines and magnified in the insets. Scale bars in full panels and zoomed panels correspond to 5 μm and 1 μm, respectively. The right-hand panel shows co-localization analysis of LC3 and phalloidin.

Interestingly, the abnormal LC3-positive structures in *Capzb* knockdown cells increased in size over time. At 8 h after starvation, LC3 was present on long tubule-like structures (Fig. 5i,j), which

were also DFCP1-positive (Fig. 5k). As DFCP1 is an ER-anchored protein⁵, these data indicate that the failure of autophagosome formation in *Capzb* knockdown cells causes accumulation

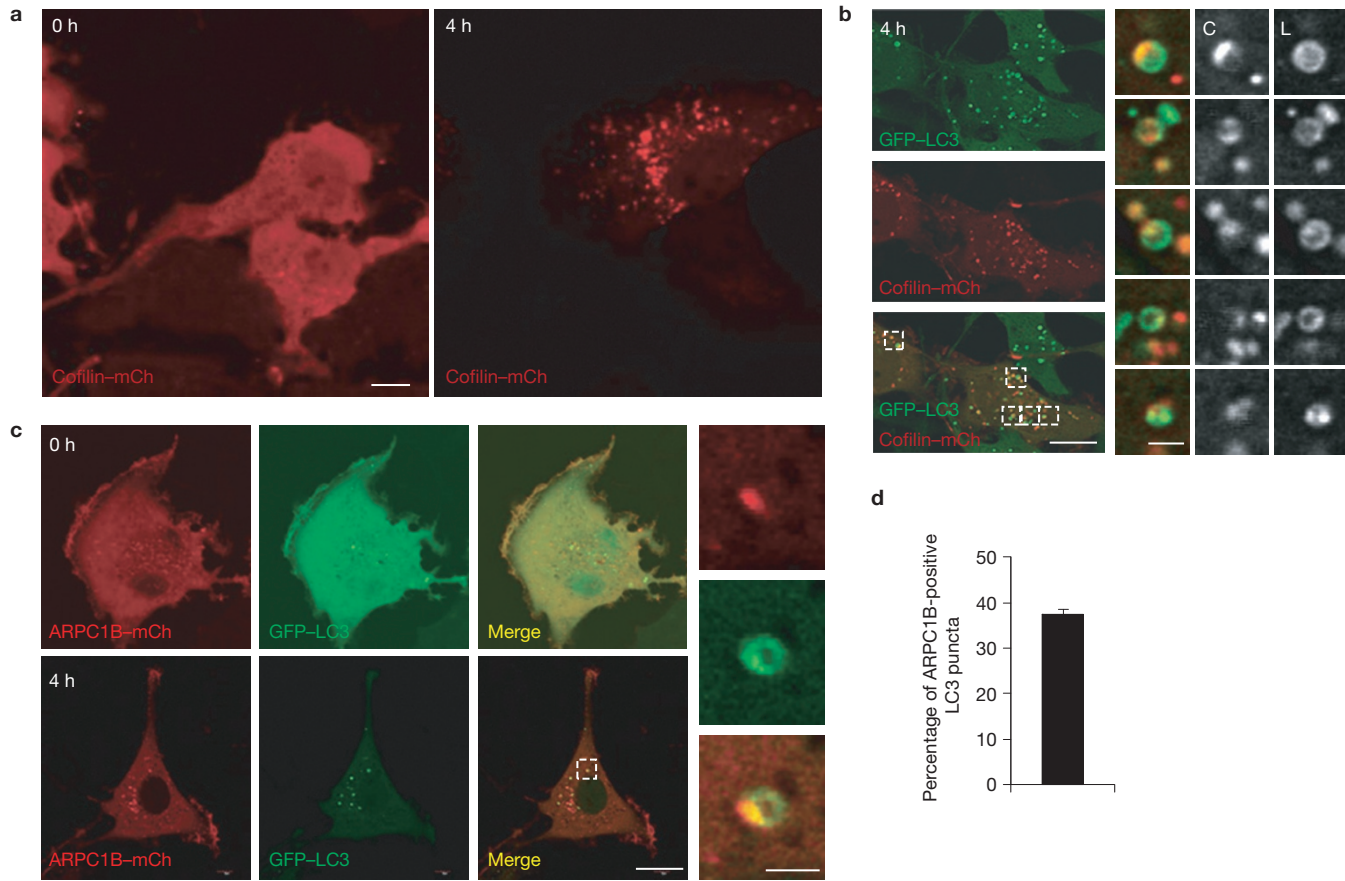


Figure 4 Actin puncta contain branched actin networks. **(a)** Cofilin–Cherry red-expressing NRK cells were starved for 0 and 4 h and cells were observed by confocal microscopy. Scale bar, 10 μ m. **(b)** NRK cells expressing Cofilin–Cherry red (C) and GFP–LC3 (L) were starved for 4 h and then observed by confocal microscopy. Regions of interest are outlined with white dashed lines and magnified to the right. Scale bars in full panels and zoomed panels correspond to 5 μ m and 1 μ m, respectively. **(c)** GFP–LC3-expressing NRK

cells transfected with ARPC1B–Cherry red were starved for 4 h and then observed by confocal microscopy. Regions of interest are outlined with white dashed lines and magnified to the right. Scale bars in full panels and zoomed panels correspond to 5 μ m and 1 μ m, respectively. **(d)** Cells from **c** were quantified for ARPC1B–Cherry red-positive LC3 puncta. ($n=3$ independent experiments; 50 cells were assessed per independent experiment). Data represent mean \pm s.d.

of LC3/DFCP1-positive membrane structures, possibly along the ER.

CapZ regulates autophagosomal membrane shaping

To better understand the role of actin and CapZ β in autophagosome formation, we more closely analysed the morphology of isolation membranes in control or *Capzb* knockdown cells. Confocal images show that isolation membranes in control cells have a unique structure, with the omegasome forming a ring-like base (DFCP1 base) from which LC3 puncta protrude to create a highly curved, dome-like structure (LC3 dome; Fig. 6a). In contrast, in *Capzb* knockdown cells, DFCP1 and LC3 are co-localized on short tubular or ring-shaped structures (Fig. 6a), with no LC3 dome extruding from the DFCP1 base. The 2D image acquired by confocal microscopy is a cross-sectional view of a 3D structure (Fig. 6a). An isolation membrane can therefore give two cross-sectional views dependent on its orientation; one is the DFCP1 base filled with LC3, and the other is the LC3 dome protruding from the DFCP1 base. In contrast, the cross-sectional views of isolation membranes that fail to form the proper shape will appear as enlarged rings or mixed tubules (Fig. 6a). Thus,

confocal images indicate that isolation membranes have defective morphology in *Capzb* knockdown cells. Three-dimensional SIM further confirmed the abnormal LC3 dome formation (Fig. 6b). Similarly, transmission electron microscopy (TEM) analysis revealed that control cells have well-defined isolation membranes surrounded by an ER ‘cradle’, whereas in *Capzb* knockdown cells, isolation membranes formed multilayer membrane mixtures that resemble a collapsed dome (Fig. 6c,d). These multilayer membrane mixtures are also observed in cells undergoing brief treatment with CK666 (Supplementary Fig. 4e,f). To validate that these multilayer membrane mixtures are indeed abnormal isolation membranes/autophagosomes, we carried out immuno-electron microscopy analysis on *Capzb* knockdown cells. We found that these multilayer membrane mixtures are LC3-positive (Fig. 6e–g), and thus are derived from isolation membranes/autophagosomes. Many of these multilayer membrane mixtures are associated with the ER, and this was further validated by electron tomography (Fig. 6h,i). In some cases, multilayer membrane mixtures were observed to connect to a mitochondrion and the ER at the same site (Fig. 6j). Using the information we gained from confocal, 3D-SIM, TEM, immuno-electron microscopy and electron

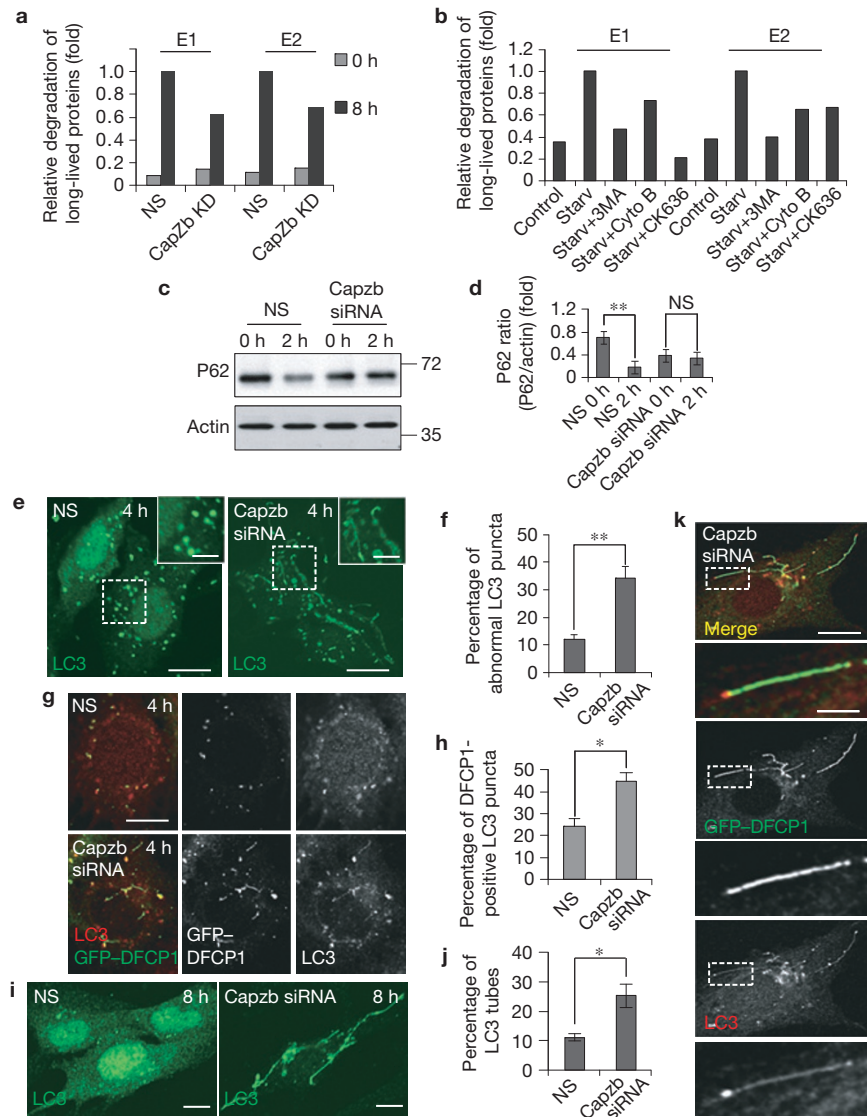


Figure 5 CapZ regulates autophagy. **(a)** NRK cells were transfected with nonspecific (NS) or *Capzb* RNAi. Cells were starved for 8 h and then examined for autophagic degradation of long-lived proteins. Three wells per sample per experiment. Data from 2 independent experiments are presented side-by-side. **(b)** NRK cells were examined for autophagic degradation of long-lived proteins after 4 h starvation. 20 mM 3-MA, 100 μ M cytochalasin B and 200 μ M CK636 were examined for their efficacy in preventing degradation. Three wells per sample per experiment. Data from 2 independent experiments are presented side-by-side. **(c)** NRK cells were transfected with nonspecific (NS) or *Capzb* RNAi. Cells were starved for 0 or 2 h and analysed by western blotting with an antibody against p62. Unprocessed original scans of blots are shown in Supplementary Fig. 9. **(d)** Western blots from **c** were quantified for the p62/actin ratio ($n=3$ independent experiments). Data represent mean \pm s.d. ** $P < 0.01$; NS, not significant (two-tailed *t*-test). **(e)** GFP-LC3-expressing NRK cells were transfected with nonspecific (NS) or *Capzb* RNAi. Cells were starved for 0 or 4 h and stained with antibody against GFP. Regions outlined with white dashed lines are magnified. Scale bars in full panels and zoomed panels correspond to 5 μ m and 2 μ m,

respectively. **(f)** Cells from **e** were quantified for abnormal tubular LC3 puncta ($n=3$ independent experiments; 50 cells were assessed per independent experiment). Data represent mean \pm s.d. ** $P < 0.01$ (two-tailed *t*-test). **(g)** GFP-DFCP1-expressing NRK cells were transfected with nonspecific (NS) or *Capzb* RNAi. Cells were starved for 0 or 4 h and stained with antibodies against GFP and LC3. Scale bar, 5 μ m. **(h)** Cells from **e** were quantified for GFP-DFCP1/LC3 double-positive puncta ($n=3$ independent experiments; 50 cells were assessed per independent experiment). Data represent mean \pm s.d. * $P < 0.05$ (two-tailed *t*-test). **(i)** GFP-LC3-expressing NRK cells were transfected with nonspecific (NS) or *Capzb* RNAi. Cells were starved for 8 h and stained with antibody against GFP. Scale bar, 10 μ m. **(j)** Cells from **h** were quantified for the percentage of LC3 tubes ($n=3$ independent experiments; 100 cells were assessed per independent experiment). Data represent mean \pm s.d. * $P < 0.05$ (two-tailed *t*-test). **(k)** GFP-DFCP1-expressing NRK cells were transfected with nonspecific (NS) or *Capzb* RNAi. Cells were starved for 8 h and stained with antibodies against GFP and LC3. Scale bar, 5 μ m. Regions outlined with white dashed lines are magnified below. Scale bars in full panels and zoomed panels correspond to 5 μ m and 2 μ m, respectively.

tomography images, we reconstructed 3D models for isolation membranes in control and *Capzb* knockdown cells. In control cells, LC3-positive membranes extrude from omegasomes to form the

dome-like isolation membrane, whereas in *Capzb* knockdown cells, the LC3-positive isolation membrane failed to generate the correct shape and instead collapsed and mixed with the omegasome (Fig. 6k).

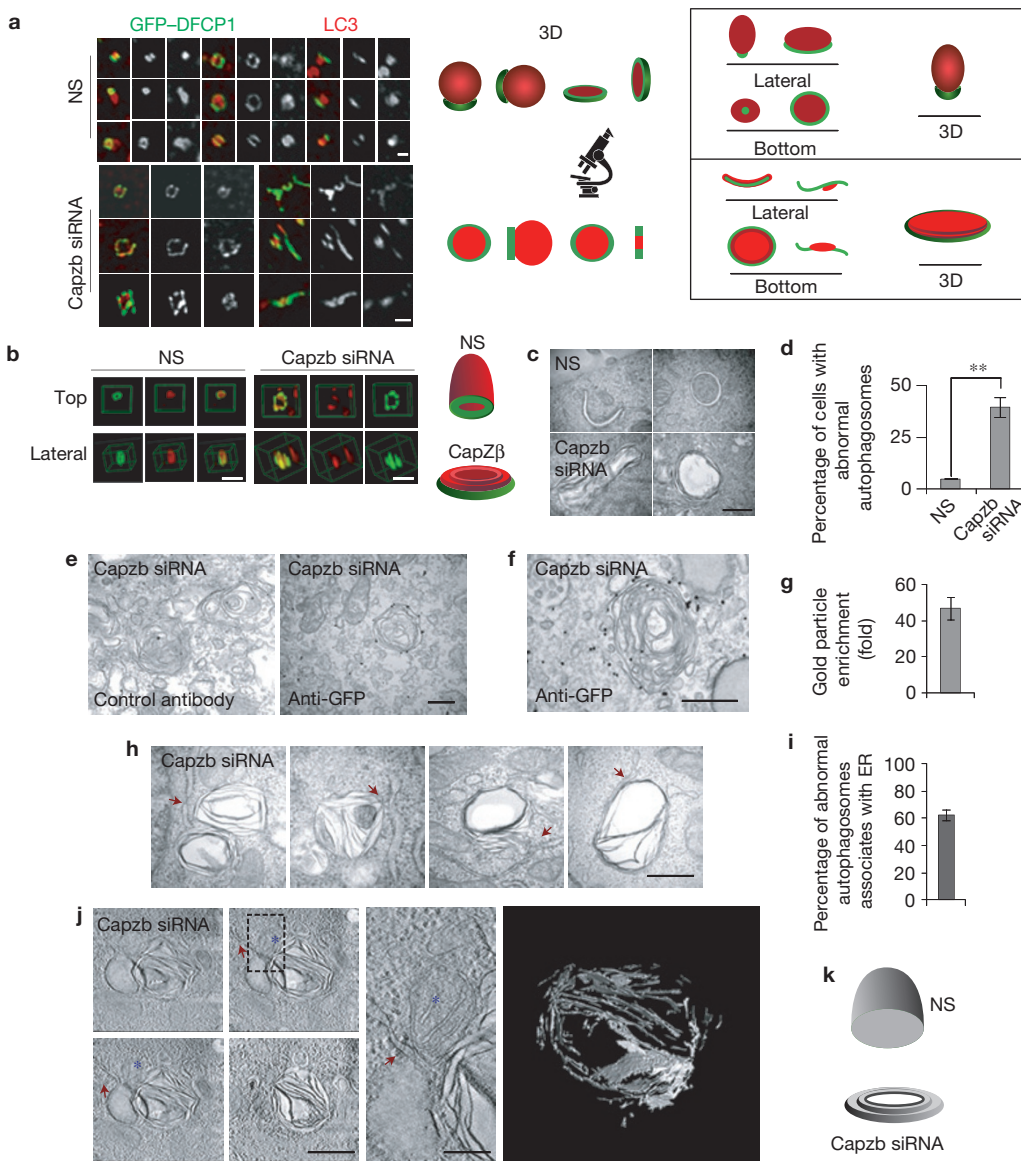


Figure 6 CapZ β regulates isolation membrane shaping. **(a)** GFP-DFCP1-expressing NRK cells were transfected with nonspecific (NS) or CapZ β RNAi. Cells were starved for 4 h and stained with antibodies against GFP and LC3. Representative confocal images of individual isolation membranes are shown on the left; scale bars, 1 μ m. Middle panel shows illustrations of cross-sectional views, visible by microscopy, of 3D structures. Right panel shows 3D models of isolation membranes, reconstructed from images in the left panel. **(b)** Cells from **a** were analysed by SIM; scale bars, 1 μ m. **(c)** NRK cells were transfected with nonspecific (NS) or CapZ β RNAi. Cells were starved for 4 h and analysed by TEM; scale bar, 500 nm. **(d)** Cells from **c** were assessed for abnormal autophagosomes in a blinded fashion and quantified ($n=3$ independent experiments; 50 cells were assessed per independent experiment). Data represent mean \pm s.d. ** $P < 0.01$ (two-tailed t -test). **(e)** GFP-LC3-expressing NRK cells were starved for 4 h and then analysed by immuno-electron microscopy using antibodies against GFP. Scale bar, 500 nm. **(f)** Representative image of an abnormal isolation

membrane/autophagosome in a cell from **e**. Scale bar, 500 nm. **(g)** The number of nanogold particles per square micrometre in cells from **e** was quantified ($n=3$ independent experiments; 10 fields were assessed per independent experiment). Data represent mean \pm s.d. **(h)** Representative images of abnormal autophagosomes from CapZ β -RNAi-transfected cells that were associated with ER. Red arrows indicate the ER. Scale bar, 500 nm. **(i)** Cells from **h** were assessed for the percentage of abnormal autophagosomes that were associated with the ER ($n=3$ independent experiments; 50 fields were assessed per independent experiment). Data represent mean \pm s.d. **(j)** Abnormal autophagosomes from CapZ β -RNAi-transfected cells were analysed by electron tomography. Blue asterisks indicate the mitochondrion; red arrows indicate the ER. Regions outlined with black dashed lines are magnified to the right. Scale bars in full panels and zoomed panels correspond to 500 nm and 200 nm, respectively. Right panel shows a 3D reconstruction of the abnormal autophagosome from the left panel. **(k)** Model of isolation membranes from NS (top) and CapZ β knockdown (bottom) cells.

CapZ and PtdIns(3)P regulate assembly of actin puncta inside isolation membranes

As knockdown of CapZ genes has been shown to abolish the formation of lamellipodia and branched networks, we next tested the effect

of CapZ knockdown on actin puncta formation. Staining with phalloidin and LC3 revealed that formation of actin puncta was markedly reduced inside isolation membranes in CapZ β knockdown NRK (Fig. 7a,b and Supplementary Fig. 5a,b), and this phenotype

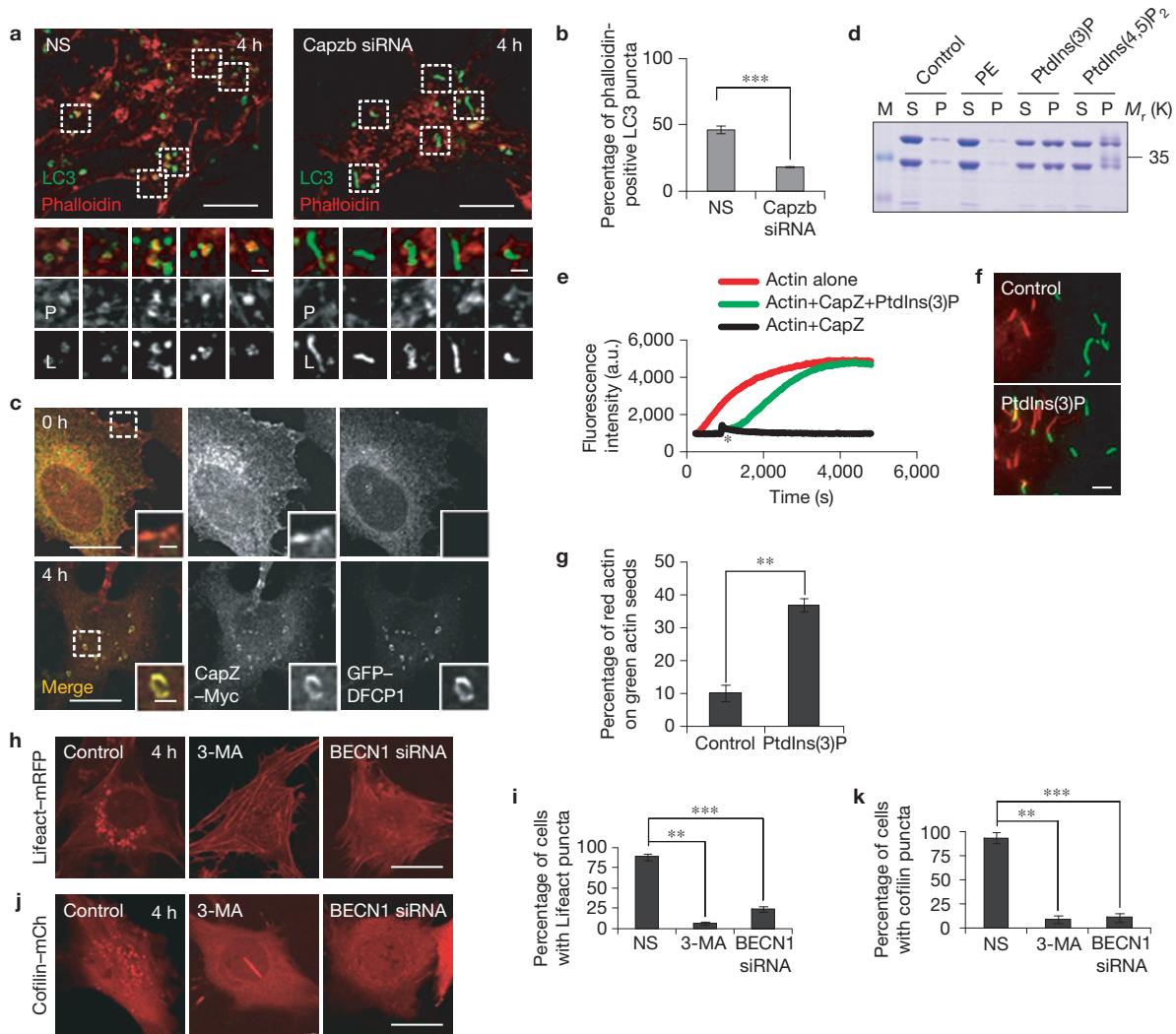


Figure 7 CapZ and PtdIns(3)P are required for actin puncta formation in isolation membranes. **(a)** NRK cells were transfected with nonspecific (NS) or *Capzb* RNAi and starved for 4 h, and then stained with antibodies against LC3 (L) and phalloidin (P). Regions outlined with white dashed lines are magnified below. Scale bars in full panels and zoomed panels correspond to 5 μm and 1 μm, respectively. **(b)** Cells from **a** were quantified for phalloidin-positive LC3 puncta ($n=3$ independent experiments; 40 cells were assessed per independent experiment). Data represent mean \pm s.d. *** $P < 0.001$ (two-tailed *t*-test). **(c)** NRK cells were transfected with GFP-DFCP1 and CapZ-Myc, then starved for 0 or 4 h, and stained with antibodies against GFP and Myc. Regions outlined with white dashed lines are magnified below. Scale bars in full panels and zoomed panels correspond to 5 μm and 1 μm, respectively. **(d)** PE or PtdIns(3)P micelles were mixed with 2 μM of dimerized CapZα and CapZβ and co-sedimented. Proteins in supernatant (S) and precipitate (P) were visualized with Coomassie brilliant blue. The experiment was repeated 3 times. Unprocessed original scans of gels are shown in Supplementary Fig. 9. **(e)** Actin polymerization reactions were initiated by mixing 1 μg ml⁻¹ spectrin-F-actin seed with pyrene-labelled actin with or without 10 nM CapZ. After 900 s, 133 μM PtdIns(3)P was added to the reaction containing CapZ. The asterisk indicates the addition of PtdIns(3)P at 900 s. **(f)** Green actin seeds that were capped by CapZ and labelled by biotin were attached to streptavidin-coated flow cell chambers. 1 μM red actin was incubated with or without 200 nM PtdIns(3)P for 20 min. Polymerization of red actin onto uncapped green actin seeds was visualized by TIRF microscopy. Scale bar, 5 μm. **(g)** The percentage of red actin polymerized onto green actin seeds from **f** was quantified ($n=3$ independent experiments; 40 fields were assessed per independent experiment). Data represent mean \pm s.d. ** $P < 0.01$ (two-tailed *t*-test). **(h)** Lifeact-mRFP-expressing NRK cells were transfected with nonspecific RNAi (Control) or *Beclin-1* RNAi (BECN1 siRNA), and then starved for 4 h with or without 3-MA. Scale bar, 5 μm. **(i)** Cells from **h** were quantified for the presence of actin puncta ($n=3$ independent experiments; 100 cells were assessed per independent experiment). Data represent mean \pm s.d. ** $P < 0.01$, *** $P < 0.001$ (two-tailed *t*-test). **(j)** Cofilin-Cherry red-expressing NRK cells were transfected with nonspecific RNAi (Control) or *Beclin-1* RNAi (BECN1 siRNA), and then starved for 4 h with or without 3-MA. Scale bar, 5 μm. **(k)** Cells from **j** were quantified for the presence of actin puncta ($n=3$ independent experiments; 60 cells were assessed per independent experiment). Data represent mean \pm s.d. ** $P < 0.01$, *** $P < 0.001$ (two-tailed *t*-test).

can be rescued by overexpression of an RNAi-resistant *Capzb* plasmid (Supplementary Fig. 5c,d).

Next, we studied the localization of CapZ complexes during autophagy. We found that when cells were grown in nutrient-rich

medium, CapZ complexes were enriched on plasma membranes, whereas 4 h after starvation, CapZ clearly co-localized with the omegasome marker DFCP1 (Fig. 7c), indicating that CapZ complexes were recruited to omegasomes. We tested whether the CapZ complex

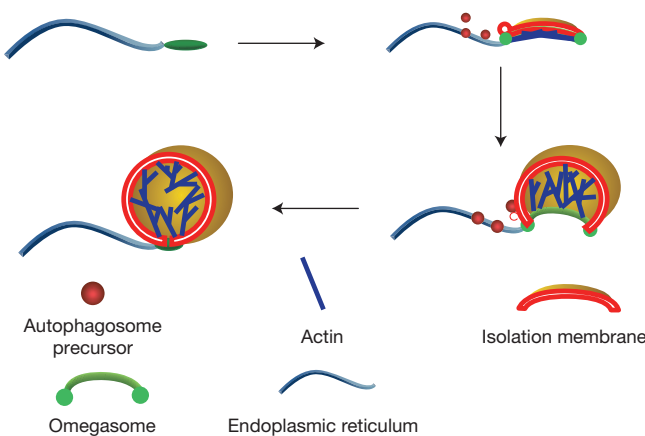


Figure 8 Provisional model of autophagosomal membrane shaping.

can interact with PtdIns(3)P, the main lipid in omegasomes⁵. Using recombinant CapZ α and CapZ β proteins purified from *Escherichia coli*, we showed that the CapZ complex can be pulled down by PtdIns(3)P and PtdIns(4,5)P₂ micelles (Fig. 7d). In contrast, a CapZ complex mutant, which has reduced PtdIns(4,5)P₂- and actin-binding ability¹⁵, showed impaired ability to bind PtdIns(3)P micelles and impaired recruitment to PtdIns(3)P-enriched omegasomes (Supplementary Fig. 6a,b). The physiological relevance of the binding between CapZ complexes and PtdIns(3)P micelles remains unclear, because CapZ complexes fail to bind liposomes containing 20% PtdIns(3)P (Supplementary Fig. 7). Nevertheless, these data raise the possibility that the recruitment of CapZ to omegasomes may occur through PtdIns(3)P.

Polyphosphoinositides such as PtdIns(4,5)P₂ and PtdIns(4)P can cause rapid disassociation of the CapZ complex from the barbed ends of actin filaments, and the ability of PtdIns(4,5)P₂ to remove capping proteins has been proposed as a potential mechanism for stimulating actin polymerization and assembly of actin-based structures around PtdIns(4,5)P₂-enriched membranes⁴⁷. Next, we tested whether PtdIns(3)P can cause polymerization of capped actin. Actin filaments were pre-capped with CapZ, which stabilizes filament length by preventing both polymerization and depolymerization at the barbed end. The capping efficiency was confirmed by reduced polymerization kinetics compared with the sharp increase in fluorescence intensity for CapZ-free filaments before 900 s (Fig. 7e). After PtdIns(3)P was added to pre-capped actin, the fluorescence intensity quickly increased and reached the same plateau as CapZ-free filaments (Fig. 7e), indicating that PtdIns(3)P caused uncapping and polymerization of actin. More detailed analysis revealed that PtdIns(3)P uncapped and polymerized actin in a concentration-dependent manner (Supplementary Fig. 8a). Compared with PtdIns(4,5)P₂, PtdIns(3)P has a weaker uncapping effect (Supplementary Fig. 8b). The uncapping effect of PtdIns(3)P on pre-capped actin was also confirmed by directly visualizing uncapping of ‘green’ actin seeds and polymerization of ‘red’ actin on these uncapped seeds by total internal reflection fluorescence (TIRF) microscopy (Fig. 7f,g). These data suggest that PtdIns(3)P may regulate actin puncta formation during autophagy.

Next, we tested whether PtdIns(3)P plays a role in actin puncta formation. We treated cells with the PtdIns(3)P inhibitor 3-MA and

found that it almost completely abolished the starvation-induced formation of actin puncta and cofilin puncta (Fig. 7h,i). To further validate the role of PtdIns(3)P in formation of actin puncta, we knocked down Beclin-1, an essential component of the Vps34 complex^{48,49}, which is required for generation of PtdIns(3)P during autophagy. Similar to 3-MA treatment, Beclin-1 knockdown markedly reduced the starvation-induced appearance of actin puncta and cofilin puncta (Fig. 7j,k). Taking these data together, we conclude that PtdIns(3)P is required on omegasomes for formation of actin puncta inside isolation membranes, possibly by stimulating localized actin polymerization through disassociation of CapZ.

DISCUSSION

One of the fundamental questions regarding autophagosome formation is how membrane curvature is generated and maintained during expansion of the isolation membrane. It is generally believed that the autophagosome is formed by fusion of vesicular precursors. As vesicle fusion usually generates a larger vesicle rather than a curved membrane cisterna, the topology of the isolation membrane indicates that there must be a mechanism to deform it into a curved structure. In this manuscript, we have reported the mechanism underlying autophagosomal membrane shaping. We found that actin filaments are depolymerized shortly after starvation; actin puncta containing branched actin networks are formed inside the centre cavity of the isolation membrane; the formation of actin puncta is dependent on PtdIns(3)P and CapZ; and the formation of the branched actin network inside the isolation membrane is required for autophagosome formation, as disrupting its assembly by knocking down the actin capping protein subunit CapZ β or brief treatment with branched actin network inhibitor CK666 causes failure of isolation membrane curvature and results in collapse of omegasomes and isolation membranes into mixed-membrane bundles. We further demonstrated that CapZ can bind PtdIns(3)P micelle, and the interaction between PtdIns(3)P and CapZ promotes actin polymerization. Our data enable us to assemble a working model of how the shape of the isolation membrane is achieved (Fig. 8). In this model, PtdIns(3)P on the omegasome promotes the localized polymerization of actin, which forms a branched actin network that serves as a scaffold and/or creates a propulsion force to generate the shape of the isolation membrane.

The actin-based cytoskeleton has been shown to play an important role in autophagy; for example, actin has also been shown to play a role at the early stage of autophagosome formation linked to PtdIns(3)P generation¹⁵. Arp2/3, the nucleator for the formation of branched actin networks, has been reported to be required for autophagosome formation by regulating the trafficking of Atg9 in yeast⁵⁰. Recently, the Arp2/3 complex has been shown to regulate autophagosome biogenesis through an actin-comet tail motility mechanism⁵¹. In this study, we also demonstrated that branched actin networks are required for autophagosomal membrane shaping. All of this evidence supports the idea that actin regulates multiple steps of autophagosome formation.

Our model also provides clues to a better understanding of the roles of PtdIns(3)P. It is well established that PtdIns(3)P, one of the essential molecules for autophagosome formation, carries out its function by recruiting PtdIns(3)P-binding proteins such as Atg18/WIPIs,

which in turn recruit core autophagy machinery components such as Atg12–Atg5–Atg16L1 (refs 49,52,53). Our data reveal another role for PtdIns(3)P: by promoting actin network formation inside isolation membranes, PtdIns(3)P plays an essential role in shaping the autophagosomal membrane.

Actin filament growth is mainly mediated by adding free actin monomers to the barbed end of actin filaments. In stable actin filaments, the actin-capping protein CapZ binds to the barbed end of actin with high affinity, blocking the addition of new actin to the filament and thus preventing actin filament growth^{54,55}. Various mechanisms can cause uncapping of the actin barbed end, which initiates actin polymerization and results in filament growth⁵⁵. For example, binding of CapZ to polyphosphoinositides such as PtdIns(4,5)P₂ has been shown to cause uncapping of CapZ from actin filaments and promote actin filament growth *in vitro*⁵⁵, and uncapping of CapZ by PtdIns(4,5)P₂ on plasma membranes has been proposed to promote actin polymerization on plasma membranes and formation of lamellipodia. In line with this model, CapZ has been shown to be required for lamellipodia formation⁵⁶. Our data suggest that similar to lamellipodia formation, the PtdIns(3)P-mediated uncapping is a possible mechanism for the temporal and spatial regulation of actin puncta formation. In this model, formation of the Vps34/Atg14/Beclin1/P150 complex generates PtdIns(3)P on omegasomes. When the local concentration of PtdIns(3)P reaches a certain level of enrichment, CapZ complexes are removed from capped actin. The uncapping of CapZ by PtdIns(3)P provides a temporal and spatial regulation for localized polymerization of actin around the omegasome, which in turn promotes autophagosomal membrane shaping.

□

METHODS

Methods and any associated references are available in the [online version of the paper](#).

Note: Supplementary Information is available in the online version of the paper

ACKNOWLEDGEMENTS

We are grateful to Nikon instruments (Shanghai) and the Tsinghua Cell Biology Core Facility for providing technical support, and to Y. Li and L. Huang for assistance with confocal microscopy, TEM, and image processing. GFP–DFCP1 was a gift from N. T. Ktistakis. This research was supported by National Science Foundation Grants 31125018, 31030043 and 31321003, 973 Program 2010CB833704, 2011CB910100, and Tsinghua University Grants 2010THZ0 and 2009THZ03071 to L.Y.

AUTHOR CONTRIBUTIONS

L.Y., Z.C. and N.M. conceived the idea. L.Y. supervised the study with help from N.M., Y.C. and Z.C. N.M. and Y.C. designed and conducted most of the experiments and analysed the data. N.G. and Q.G. helped with the tomography study. S.W., M.C., M.Z., G.Y., M.M., Q.S., S.L., J.S., Y.S. and J.X. contributed to the experiments. L.Y. and Y.C. wrote the manuscript.

COMPETING FINANCIAL INTERESTS

The authors declare no competing financial interests.

Published online at <http://dx.doi.org/10.1038/ncb3215>

Reprints and permissions information is available online at www.nature.com/reprints

- Klionsky, D. J. & Emr, S. D. Autophagy as a regulated pathway of cellular degradation. *Science* **290**, 1717–1721 (2000).
- Klionsky, D. J. The molecular machinery of autophagy: unanswered questions. *J. Cell Sci.* **118**, 7–18 (2005).
- Lum, J. J., DeBerardinis, R. J. & Thompson, C. B. Autophagy in metazoans: cell survival in the land of plenty. *Nat. Rev. Mol. Cell Biol.* **6**, 439–448 (2005).
- Mizushima, N., Ohsumi, Y. & Yoshimori, T. Autophagosome formation in mammalian cells. *Cell Struct. Funct.* **27**, 421–429 (2002).
- Axe, E. L. *et al.* Autophagosome formation from membrane compartments enriched in phosphatidylinositol 3-phosphate and dynamically connected to the endoplasmic reticulum. *J. Cell Biol.* **182**, 685–701 (2008).
- Hayashi-Nishino, M. *et al.* A subdomain of the endoplasmic reticulum forms a cradle for autophagosome formation. *Nat. Cell Biol.* **11**, 1433–1437 (2009).
- Roberts, R. & Ktistakis, N. T. Omegasomes: PI3P platforms that manufacture autophagosomes. *Essays Biochem.* **55**, 17–27 (2013).
- Seglen, P. O., Gordon, P. B. & Holen, I. Non-selective autophagy. *Semin. Cell Biol.* **1**, 441–448 (1990).
- Mizushima, N. Autophagy: process and function. *Genes Dev.* **21**, 2861–2873 (2007).
- Kirchhausen, T., Owen, D. & Harrison, S. C. Molecular structure, function, and dynamics of clathrin-mediated membrane traffic. *Cold Spring Harb. Perspect. Biol.* **6**, a016725 (2014).
- Shibutani, S. T. & Yoshimori, T. A current perspective of autophagosome biogenesis. *Cell Res.* **24**, 58–68 (2014).
- Chhabra, E. S. & Higgs, H. N. The many faces of actin: matching assembly factors with cellular structures. *Nat. Cell Biol.* **9**, 1110–1121 (2007).
- Pollard, T. D., Blanchard, L. & Mullins, R. D. Molecular mechanisms controlling actin filament dynamics in nonmuscle cells. *Annu. Rev. Biophys. Biomol. Struct.* **29**, 545–576 (2000).
- Small, J. V. *et al.* Unravelling the structure of the lamellipodium. *J. Microsc.* **231**, 479–485 (2008).
- Aguilera, M. O., Beron, W. & Colombo, M. I. The actin cytoskeleton participates in the early events of autophagosome formation upon starvation induced autophagy. *Autophagy* **8**, 1590–1603 (2012).
- Aplin, A., Jasionowski, T., Tuttle, D. L., Lenk, S. E. & Dunn, W. A. Cytoskeletal elements are required for the formation and maturation of autophagic vacuoles. *J. Cell Physiol.* **152**, 458–466 (1992).
- Yu, L. *et al.* Termination of autophagy and reformation of lysosomes regulated by mTOR. *Nature* **465**, 942–946 (2010).
- Barak, L. S., Yocum, R. R. & Webb, W. W. *In vivo* staining of cytoskeletal actin by autointernalization of nontoxic concentrations of nitrobenzoxadiazole–phallacidin. *J. Cell Biol.* **89**, 368–372 (1981).
- Kabeya, Y. *et al.* LC3, a mammalian homologue of yeast Apg8p, is localized in autophagosome membranes after processing. *EMBO J.* **19**, 5720–5728 (2000).
- Riedl, J. *et al.* Lifeact: a versatile marker to visualize F-actin. *Nat. Methods* **5**, 605–607 (2008).
- Derubeis, A. R., Young, M. F., Jia, L., Robey, P. G. & Fisher, L. W. Double FYVE-containing protein 1 (DFCP1): isolation, cloning and characterization of a novel FYVE finger protein from a human bone marrow cDNA library. *Gene* **255**, 195–203 (2000).
- Cheung, P. C., Trinkle-Mulcahy, L., Cohen, P. & Lucocq, J. M. Characterization of a novel phosphatidylinositol 3-phosphate-binding protein containing two FYVE fingers in tandem that is targeted to the Golgi. *Biochem. J.* **355**, 113–121 (2001).
- Ridley, S. H. *et al.* FENS-1 and DFCP1 are FYVE domain-containing proteins with distinct functions in the endosomal and Golgi compartments. *J. Cell Sci.* **114**, 3991–4000 (2001).
- Gustafsson, M. G. L. Surpassing the lateral resolution limit by a factor of two using structured illumination microscopy. *J. Microsc.* **198**, 82–87 (2000).
- Klionsky, D. J., Elazar, Z., Seglen, P. O. & Rubinsztein, D. C. Does bafilomycin A1 block the fusion of autophagosomes with lysosomes? *Autophagy* **4**, 849–950 (2008).
- Hawkins, M., Pope, B., Maciver, S. K. & Weeds, A. G. Human actin depolymerizing factor mediates a pH-sensitive destruction of actin filaments. *Biochemistry* **32**, 9985–9993 (1993).
- Hayden, S. M., Miller, P. S., Brauweiler, A. & Bamburg, J. R. Analysis of the interactions of actin depolymerizing factor with G- and F-actin. *Biochemistry* **32**, 9994–10004 (1993).
- Yonezawa, N., Nishida, E. & Sakai, H. pH control of actin polymerization by cofilin. *J. Biol. Chem.* **260**, 14410–14412 (1985).
- Moon, A. & Drubin, D. G. The ADF/cofilin proteins: stimulus-responsive modulators of actin dynamics. *Mol. Biol. Cell* **6**, 1423–1431 (1995).
- Theriot, J. A. Accelerating on a treadmill: ADF/cofilin promotes rapid actin filament turnover in the dynamic cytoskeleton. *J. Cell Biol.* **136**, 1165–1168 (1997).
- Svitkina, T. M. & Borisy, G. G. Arp2/3 complex and actin depolymerizing factor cofilin in dendritic organization and treadmilling of actin filament array in lamellipodia. *J. Cell Biol.* **145**, 1009–1026 (1999).
- Yamaguchi, H. *et al.* Molecular mechanisms of invadopodium formation: the role of the N-WASP-Arp2/3 complex pathway and cofilin. *J. Cell Biol.* **168**, 441–452 (2005).
- Bailly, M. *et al.* The F-actin side binding activity of the Arp2/3 complex is essential for actin nucleation and lamellipod extension. *Curr. Biol.* **11**, 620–625 (2001).
- Nolen, B. J. *et al.* Characterization of two classes of small molecule inhibitors of Arp2/3 complex. *Nature* **460**, 1031–1034 (2009).
- Goley, E. D. & Welch, M. D. The ARP2/3 complex: an actin nucleator comes of age. *Nat. Rev. Mol. Cell Biol.* **7**, 713–726 (2006).
- Higgs, H. N. & Pollard, T. D. Regulation of actin filament network formation through ARP2/3 complex: activation by a diverse array of proteins. *Annu. Rev. Biochem.* **70**, 649–676 (2001).

37. Mullins, R. D., Heuser, J. A. & Pollard, T. D. The interaction of Arp2/3 complex with actin: nucleation, high affinity pointed end capping, and formation of branching networks of filaments. *Proc. Natl Acad. Sci. USA* **95**, 6181–6186 (1998).
38. Welch, M. D., DePace, A. H., Verma, S., Iwamatsu, A. & Mitchison, T. J. The human Arp2/3 complex is composed of evolutionarily conserved subunits and is localized to cellular regions of dynamic actin filament assembly. *J. Cell Biol.* **138**, 375–384 (1997).
39. Chhabra, E. S. & Higgs, H. N. The many faces of actin: matching assembly factors with cellular structures. *Nat. Cell. Biol.* **9**, 1110–1121 (2007).
40. Cooper, J. A. & Schafer, D. A. Control of actin assembly and disassembly at filament ends. *Curr. Opin. Cell Biol.* **12**, 97–103 (2000).
41. Carlier, M. F. & Pantaloni, D. Control of actin assembly dynamics in cell motility. *J. Biol. Chem.* **282**, 23005–23009 (2007).
42. Cooper, J. A. & Sept, D. New insights into mechanism and regulation of actin capping protein. *Int. Rev. Cell Mol. Biol.* **267**, 183–206 (2008).
43. Heiss, S. G. & Cooper, J. A. Regulation of CapZ, an actin capping protein of chicken muscle, by anionic phospholipids. *Biochemistry* **30**, 8753–8758 (1991).
44. Hug, C., Miller, T. M., Torres, M. A., Casella, J. F. & Cooper, J. A. Identification and characterization of an actin-binding site of CapZ. *J. Cell Biol.* **116**, 923–931 (1992).
45. Chen, R. *et al.* The general amino acid control pathway regulates mTOR and autophagy during serum/glutamine starvation. *J. Cell Biol.* **206**, 173–182 (2014).
46. Bjorkoy, G. *et al.* p62/SQSTM1 forms protein aggregates degraded by autophagy and has a protective effect on huntingtin-induced cell death. *J. Cell Biol.* **171**, 603–614 (2005).
47. Schafer, D. A., Jennings, P. B. & Cooper, J. A. Dynamics of capping protein and actin assembly *in vitro*: uncapping barbed ends by polyphosphoinositides. *J. Cell Biol.* **135**, 169–179 (1996).
48. Liang, X. H. *et al.* Induction of autophagy and inhibition of tumorigenesis by beclin 1. *Nature* **402**, 672–676 (1999).
49. Furuya, N., Yu, F., Byfield, M., Pattingre, S. & Levine, B. The evolutionarily conserved domain of Beclin 1 is required for Vps34 binding, autophagy and tumor suppressor function. *Autophagy* **1**, 46–52 (2005).
50. Monastyrskaya, I. *et al.* Arp2 links autophagic machinery with the actin cytoskeleton. *Mol. Biol. Cell* **19**, 1962–1975 (2008).
51. Kast, D. J., Zajac, A. L., Holzbaur, E. L., Ostap, E. M. & Dominguez, R. WHAMM directs the Arp2/3 complex to the ER for autophagosome biogenesis through an actin comet tail mechanism. *Curr. Biol.* **25**, 1791–1797 (2015).
52. Proikas-Cezanne, T., Takacs, Z., Donnes, P. & Kohlbacher, O. WIPI proteins: essential PtdIns3P effectors at the nascent autophagosome. *J. Cell Sci.* **128**, 207–217 (2015).
53. Baskaran, S., Ragusa, M. J. & Hurley, J. H. How Atg18 and the WIPIs sense phosphatidylinositol 3-phosphate. *Autophagy* **8**, 1851–1852 (2012).
54. Pollard, T. D. & Cooper, J. A. Actin, a central player in cell shape and movement. *Science* **326**, 1208–1212 (2009).
55. Cooper, J. A. & Schafer, D. A. Control of actin assembly and disassembly at filament ends. *Curr. Opin. Cell Biol.* **12**, 97–103 (2000).
56. Cooper, J. A. & Sept, D. New insights into mechanism and regulation of actin capping protein. *Int. Rev. Cell Mol. Biol.* **267**, 183–206 (2008).

METHODS

Cell culture, RNAi, plasmids and transfection. Normal rat kidney (NRK) cells and Raw cells were obtained from the American Type Culture Collection (ATCC) and cultured in DMEM (Hyclone) medium supplemented with 10% FBS. DMEM medium (–glutamine, Hyclone) was used as the starvation medium and was added to the dish after washing twice with PBS. Cells were transfected with 200 pmol siRNA or 2 µg DNA via Amaxanucleofection using solution T and program X-001. Cells are routinely tested for mycoplasma contamination. All cells used in this manuscript were purchased from ATCC. The cell lines were not identified through standard methods, for example short tandem repeat profiling. However, the morphology of the cells looked correct.

Antibodies and dyes. The following primary antibodies were used: mouse anti-GFP (Roche, 11814460001, 1:500), rabbit anti-LC3 (MBL, PM036, PM046, 1:500), rabbit anti-P62 (MBL, PM045, 1:1,000), rabbit anti-GFP (Invitrogen, A11122, 1:500), and rabbit anti-actin (Sigma, A2066, 1:100,000). Secondary antibodies were purchased from Invitrogen (Alexa Fluor 488 goat anti-rabbit IgG: A11008; Alexa Fluor 546 goat anti-rabbit IgG: A11035; Alexa Fluor 488 goat anti-mouse IgG: A10680; Alexa Fluor 546 goat anti-mouse IgG: A11003, 1:500). Acti-stain 535 Phalloidin (Rhodamine phalloidin, 1:50) (PHDR1), Acti-stain 555 (PHDH1, 1:50), Acti-stain 670 (PHDN1, 1:50), and rabbit skeletal muscle actin (AB07-A) were purchased from Cytoskeleton.

Live-cell imaging. Transfected cells were re-plated in Lab Tek Chambered cover glasses (NUNC) the night before imaging, and cells were maintained at 37 °C with 5% CO₂ in a LCI chamber (LCI). Images were acquired by an Olympus FV-1000 confocal microscope. All living-cell imaging experiments were repeated at least for 3 times.

Staining. Cells were washed with phosphate buffered saline (PBS), fixed in 4% paraformaldehyde for 10 min, and then washed with PBS three times for ten minutes each. Cells were permeabilized by incubating for 10 min in PBS containing 0.1% saponin. After blocking with goat serum in PBS for 30 min, cells were stained with primary antibody in blocking buffer for 1 h, and washed with PBS three times. Cells were then stained with conjugated secondary antibody in PBS for 1 h and washed with PBS three times. All statistical data of staining samples were derived from at least 3 independent experiments. The sample size and statistical test are indicated in the figure legends.

Semi-intact treatment. Semi-intact cells were prepared as described previously⁵⁷. Cells were washed with cold phosphate buffered saline (PBS). Then cells were permeabilized with 25 µg ml⁻¹ digitonin in cold buffer 1 (25 mM HEPES-KOH (pH = 7.2), 125 mM potassium acetate, 5 mM magnesium acetate, 1 mM dithiothreitol, 1 mg ml⁻¹ D-glucose) for 5 min on ice. Cells were washed with buffer 1 and incubated with buffer 1 for 20 min on ice. Then cells were fixed with 4% paraformaldehyde for 10 min at room temperature followed by a staining procedure.

Electron microscopy and immuno-electron microscopy. Cells were fixed in 2.5% glutaraldehyde in 0.1 M MOPS buffer (pH 7.0) for 8 h at room temperature, and then 2.5% glutaraldehyde/1% paraformaldehyde in 0.1 M MOPS buffer (pH 7.0) for 16 h at 4 °C. They were then post-fixed in 1% osmium tetroxide for 1 h, embedded in Spurr's resin, sectioned, doubly stained with uranyl acetate and lead citrate, and analysed using a Zeiss EM 10 transmission electron microscope.

The pre-embedding gold enhancement immunogold method was performed as described previously with a slight modification⁵⁸. In brief, cells were fixed in 4% paraformaldehyde for 30 min at room temperature. Cells were permeabilized in PBS containing 0.1% saponin for 10 min, blocked for 30 min in normal goat serum, and then exposed overnight to primary antibodies in blocking solution. GFP antibody used for immuno-electron microscopy is from Invitrogen (Catalogue no. A-11122, 1:500) and washed with PBS three times. The specimens were incubated with colloidal gold (1.4-nm-diameter, Nanoprobes, no. 7404, 1:500)-conjugated goat anti-rabbit Fab' in blocking solution for 1 h, and washed with PBS three times. Then the signal was intensified with a gold enhancement kit (GoldEnhance EM, Nanoprobes, no. 2114) for 2 min at room temperature. The specimens were post-fixed in 1% OsO₄ containing 1.5% potassium ferrocyanide, then dehydrated in a series of graded ethanol solutions and embedded in epoxy resin. Ultrathin sections were collected and stained with uranyl acetate and lead citrate and observed and analysed using a Zeiss EM 10 transmission electron microscope. All TEM-related experiments were repeated 3 times.

Electron tomography. Cells were fixed with 2.5% glutaraldehyde in 0.1 M sodium phosphate buffer (pH = 7.2) at room temperature for 2 h and then washed with the same buffer 3 times. After dehydration with a gradient of ethanol, the cells were infiltrated and embedded in SPI-Pon812. For morphology study, sections were cut

into 70 nm on an ultramicrotome (Leica EM UC7) and mounted on Formvar-coated copper grids. The sections were stained with uranyl acetate and lead citrate, and images were collected under a TEM (Hitachi H-7650) at 80 kV. For electron tomography study, sections were cut into 250 nm thick and mounted on the Formvar- and carbon-coated copper grids. After staining, the grids were examined in a TEM (FEI T12 Sprit) at 120 kV, and images (\times 20,000 magnification) were collected using FEI tomography acquisition software with 1° intervals over a tilt range of \pm 60° on a 4k \times 4k Gatan CCD (charge-coupled device) camera (Model 895 Ultra Scan 4000). The IMOD software package⁵⁹ was used for 3D reconstruction from the tilt series⁵⁹. First tilt series were binned to 1k \times 1k with a factor of 4, and then fiducial-less alignment was performed by patch tracking. Final tomograms were reconstructed from these aligned tilt series using the simultaneous iterative reconstruction technique (SIRT) algorithm. The reconstructed structures were further binned with a factor of two and low-pass filtered in Chimera to generate the final models. Electron tomography was repeated 3 times using independent RNAi knockdown.

CapZ purification. CapZ (α 1 β 2, *Mus musculus*) cDNA with a His-tag linked to the amino terminus of the α -subunit was cloned into the pET-3d vector and transformed into Rosetta (DE3) pLysS-competent *E. coli* cells (Novagen). Cells were grown in LB medium with 100 µg ml⁻¹ ampicillin and 34 µg ml⁻¹ chloramphenicol, and expression was induced at $D_{600\text{nm}}$ 0.8–1.0 with 0.5 mM isopropyl β -D-1-thiogalactopyranoside at 37 °C for 3 h. Cells were collected using a cell disrupter (ATS) in lysis buffer (50 mM Tris pH 8.0, 150 mM NaCl, 2 mM phenylmethylsulphonyl fluoride). Cell debris was sedimented at 18,000 r.p.m. in a J-20 rotor (Beckman Coulter) for 1 h. The supernatant was mixed with 5 ml nickel-Sepharose (GE) at 4 °C for 2 h. The resin was washed with washing buffer (50 mM Tris pH 8.0, 150 mM NaCl, 25 mM imidazole). CapZ was eluted with elution buffer (20 mM Tris pH 8.0, 150 mM NaCl, 200 mM imidazole). The eluted fraction was further purified on 15Q Sepharose (GE Healthcare) and a Hiprep 26/60 desalting column (GE Healthcare).

Fluorescence uncapping assay. The PtdIns(3)P uncapping assay was a modification of a previously published PtdIns(4,5)P₂-mediated uncapping assay⁶⁰. 2 µM pyrene-labelled actin (5%) was used for the uncapping assay. The polymerization buffer 10% KMEI (5 mM KCl, 0.2 mM MgCl₂, 0.1 mM EGTA, 1 mM imidazole pH 7.0), was determined to be optimal for PtdIns(3)P-mediated uncapping. The reaction was initiated by adding 1 µg ml⁻¹ spectrin-F-actin seed and 10 nM CapZ to pyrene-labelled actin in 10% KMEI buffer. 133 µM PtdIns(3)P and PtdIns(3)P buffer were added to pre-capped actin filaments 900 s after incubation and the fluorescence was monitored for a total of 4,800 s at 25 °C. The fluorescence uncapping assay was repeated 3 times. Figure 5d shows the result from one repeat.

TIRF uncapping assay. Actin was prepared from rabbit skeletal muscle acetone powder, and then polymerized in F-buffer (10 mM Tris pH 7.5, 50 mM KCl, 2 mM MgCl₂, 0.2 mM ATP) for labelling. Polymerized actin was labelled with BODIPY TMR C5 maleimide and BODIPY FL C1-iodoacetamide (Invitrogen) at Cys 374 to produce red and green F-actin, which was depolymerized in G-buffer (2 mM Tris pH 7.5, 0.1 mM CaCl₂, 0.2 mM ATP, 0.5 mM dithiothreitol) for three days to yield monomeric labelled actin. 5 µM green actin (label efficiency 12%) was incubated with 0.2 µM biotin-labelled actin (Cytoskeleton) and 1 µg ml⁻¹ spectrin-F-actin seed and polymerized in KMEI buffer (50 mM KCl, 2 mM MgCl₂, 1 mM EGTA, 10 mM imidazole pH 7.0, 0.5 mM dithiothreitol, 0.2 mM ATP, 0.1% methylcellulose, 1 mg ml⁻¹ BSA) at 37 °C for 20 min. To terminate polymerization, 50 nM CapZ was added and incubated at room temperature for 5 min. The capped green actin filaments that are labelled with biotin were loaded onto flow cell chambers and incubated at room temperature for 2 min to allow the labelled actin to attach to the streptavidin-coated surface. Samples were washed with KMEI buffer supplemented with 200 µM PtdIns(3)P to uncap CapZ from the actin filaments. 1 µM red actin (labelling efficiency 32%) was incubated with 200 µM PtdIns(3)P in KMEI buffer and immediately loaded onto flow cell chambers. For control experiments, the flow chamber was first washed with washing buffer and red actin was loaded without PtdIns(3)P. Red actin was incubated in flow cell chambers at room temperature for 20 min. Samples were observed with excitation beams at 488 nm for green actin and 532 nm for red actin. Experiments were repeated 3 times.

Liposome or micelle preparation. POPC, DOPE, PtdIns(3)P and PtdIns(4,5)P₂ were purchased from Avanti. The lipids were mixed in a glass tube and dried under vacuum for 6 h. The dried lipids were resuspended with 20 mM Hepes (pH = 7.5) and incubated at 37 °C for 30 min followed by 10 cycles of freeze and thaw. Then the suspension was subjected to 21 passages through a 100 nm Nuclepore polycarbonate membrane (Whatman). For micelle preparation, the lipid resuspension was sonicated using 30% voltage for 4 min, with a one minute pause every other minute using a sonicator (VCX105). Final liposome or micelle concentration was 1 mM.

Liposome binding assay. 2 μM of protein was incubated with 500 μM liposomes in no-salt buffer (20 mM Hepes, pH = 7.5) for Cofilin or F-buffer (2 mM Tris-HCl, pH = 8.0, 50 mM KCl, 2 mM MgCl₂, 0.5 mM dithiothreitol, 1 mM ATP) for CapZ. Reaction was carried out by incubation at room temperature for 10 min and then was sedimented at 100,000 r.p.m. in a Beckman Coulter TLA 100 rotor at 4 °C for 60 min. Supernatant was removed thoroughly, and sedimented liposomes were solubilized in 1xSDS. Equal amount of each fraction was subjected to SDS-PAGE and analysis by Coomassie brilliant blue. The experiment was repeated 3 times.

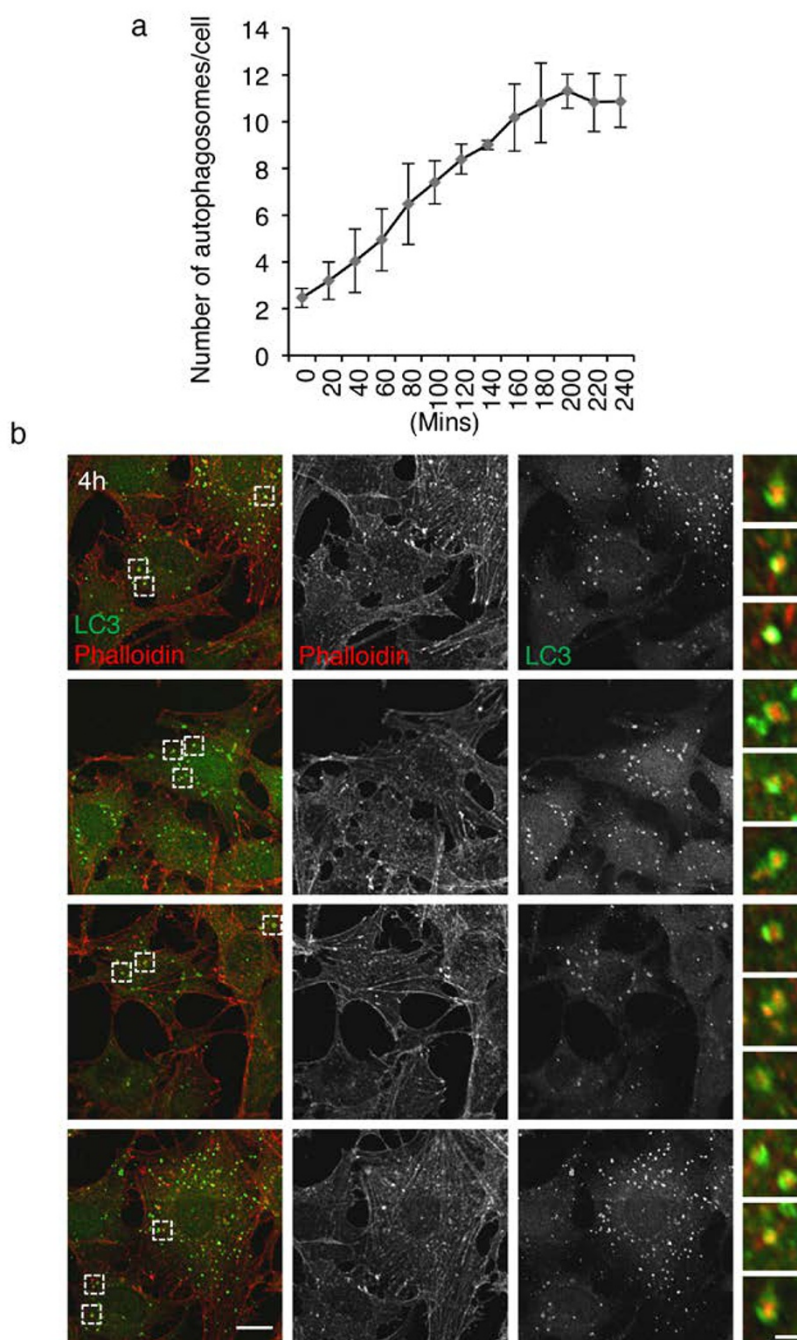
siRNA sequence. The siRNA sequence targeting rat CapZβ is 5'-GCTGAATG AGATCTACTT-3' and 5'-GGATGGTGTCTCTCGAAGA-3'; targeting mouse CapZβ is 5'-GCTGAATGAGATCTACTTT-3'; targeting rat Beclin1 is 5'-GGATG GTGTCTCTCGAAGA-3'; NS siRNA sequence is 5'-UUCUCCGAACGUGUCAC GUTT-3'; The shRNA sequence targeting rat CapZβ is 5'-GCTGAATGAGATCTA CTTT-3'.

Plasmid sequence. The plasmid constructs rat CFP-LC3 and human GFP-LC3 were provided by J. Lippincott-Schwartz's laboratory; the Lifeact-mRFPuby

was provided by W. Liu's laboratory. The human GFP-DFCP1 was provided by N. T. Ktistakis's group. Mouse His-CapZβ-CapZα was provided by Z. Chen's laboratory. His-CapZβ2(R225A)-CapZα (K256A, R260A), CapZβ-Myc, rat cofilin-mcherry and rat Arpc1-mcherry were constructed in this study.

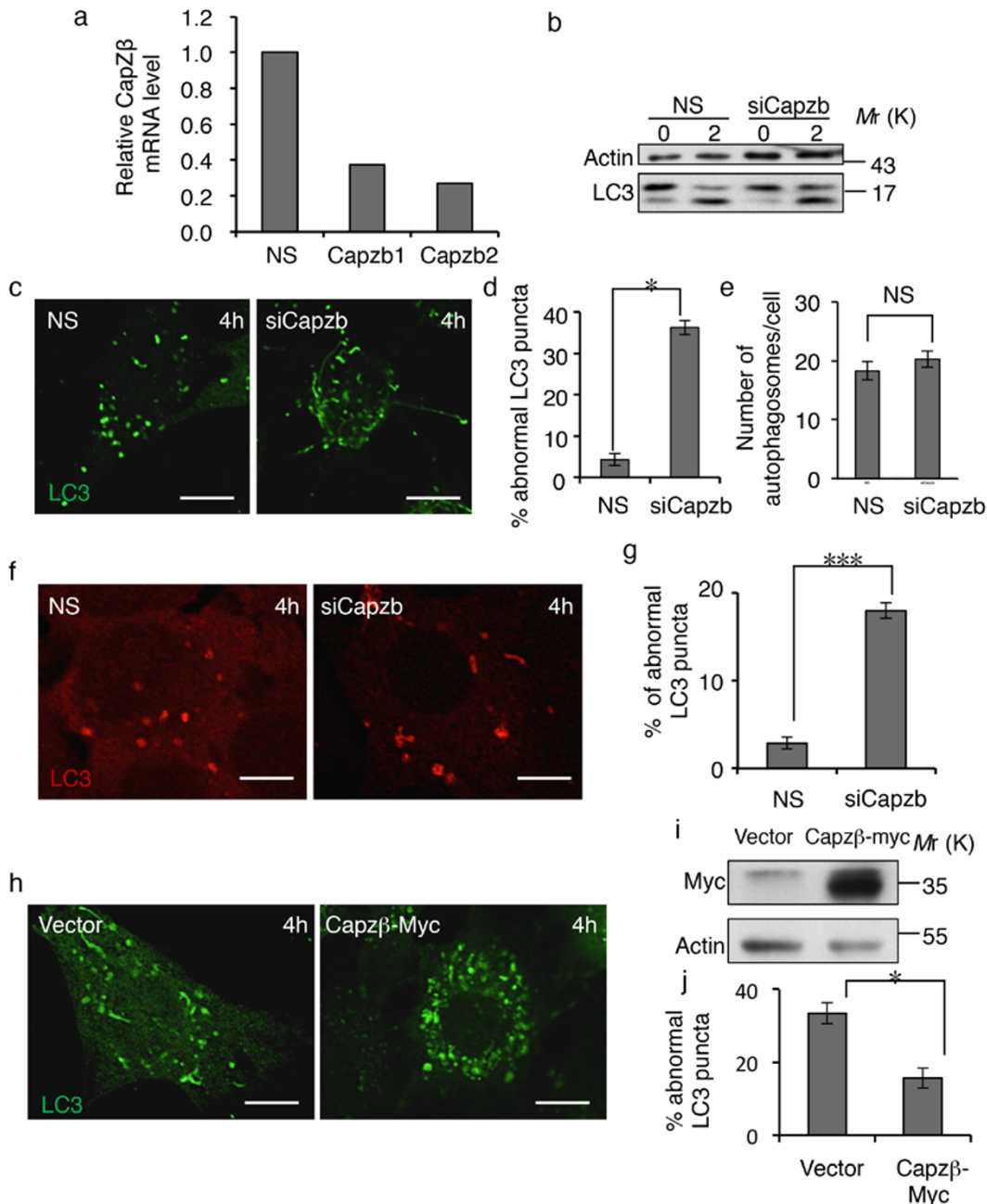
Statistics. Experimental groups were compared using two-tailed *t*-tests.

57. Plutner, H., Davidson, H. W., Saraste, J. & Balch, W. E. Morphological analysis of protein transport from the ER to Golgi membranes in digitonin-permeabilized cells: role of the P58 containing compartment. *J. Cell Biol.* **119**, 1097–1116 (1992).
58. Hayashi-Nishino, M. et al. A subdomain of the endoplasmic reticulum forms a cradle for autophagosome formation. *Nat. Cell Biol.* **11**, 1433–1437 (2009).
59. Kremer, J. R., Mastronarde, D. N. & McIntosh, J. R. Computer visualization of three-dimensional image data using IMOD. *J. Struct. Biol.* **116**, 71–76 (1996).
60. Schafer, D. A., Jennings, P. B. & Cooper, J. A. Dynamics of capping protein and actin assembly *in vitro*: uncapping barbed ends by polyphosphoinositides. *J. Cell Biol.* **135**, 169–179 (1996).



Supplementary Figure 1 Actin puncta are co-localized with LC3 puncta. (a) GFP-LC3 expressing NRK cells were starved for 4 hours and time-lapse images were acquired with a NIKON A1 confocal microscope. The number of autophagosomes at the indicated time points was quantified. (n=3 independent experiments; 50 cells per time point were assessed per

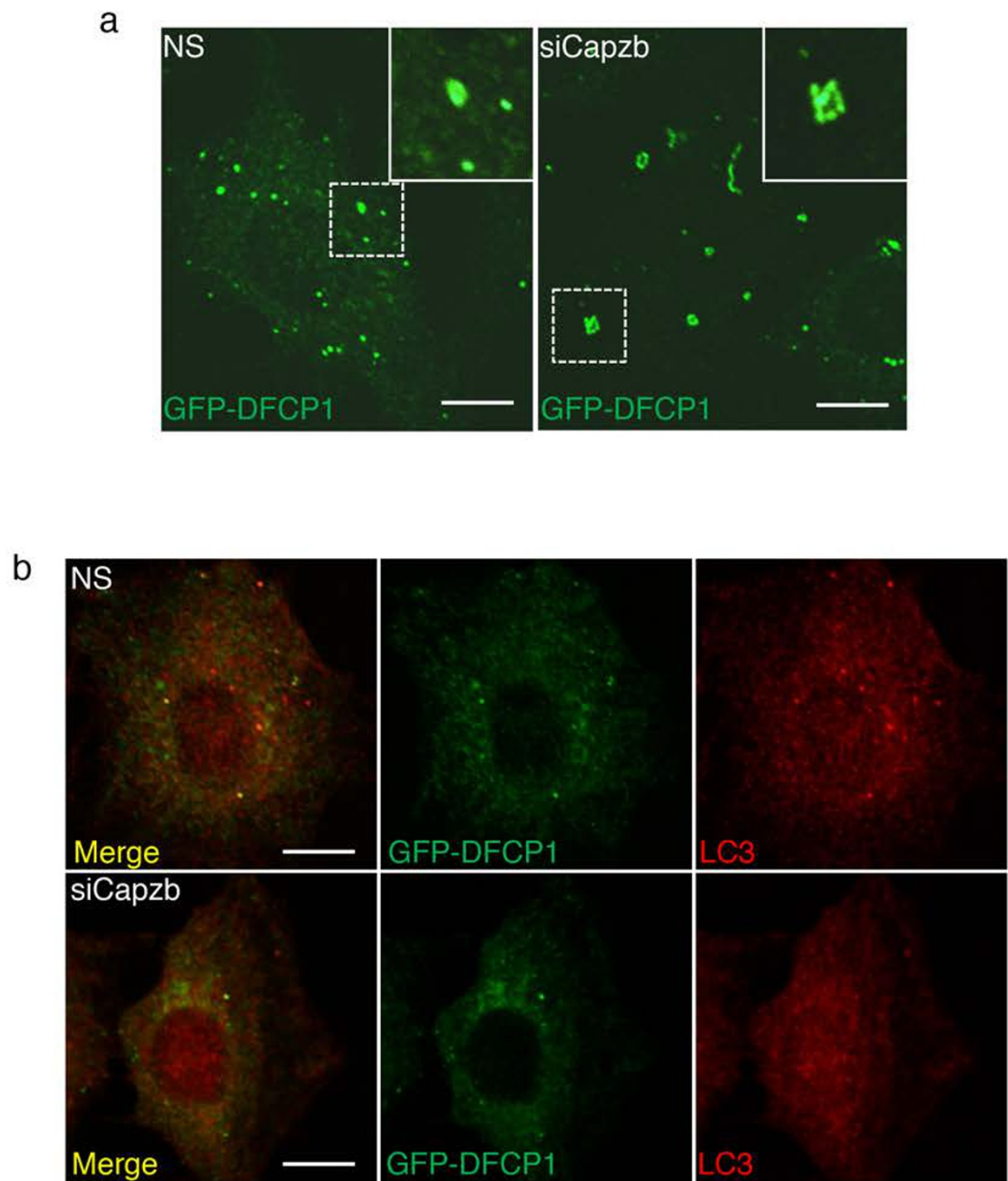
independent experiment.)Data represent mean±s.d. (b) NRK cells were starved for 4 hours then stained with phalloidin (to detect polymerized actin) and antibody to LC3. Regions of LC3 puncta that colocalize with phalloidin are outlined with white dashed lines and are magnified to the right. Scale bars in full panels and zoomed panels correspond to 5 μm and 1 μm, respectively.



Supplementary Figure 2 CapZ regulates autophagy. (a) RNAi knockdown efficiency for *Capzb*. Cells were transfected with non-specific (NS) RNAi or two different RNAis against the *Capzb* gene. 60 hours after transfection, the *Capzb* mRNA level was measured by qPCR. Data shown are from one experiment. The experiment was repeated 3 times. (b) NRK cells were transfected with nonspecific- (NS) or *Capzb*-RNAi. Cells were starved for 0 or 2 hours and analyzed by western blot with an antibody to actin or LC3. Uncropped images of blots are shown in Supplementary Fig. 9. (c) NRK cells were transfected with nonspecific- (NS) or *Capzb*-RNAi-2. Cells were starved for 4 hours and stained with antibody to LC3. Scale bar, 5 μ m. (d) Cells from (c) were assessed for abnormal tubular LC3 puncta in a blinded fashion and quantified. (n=3 independent experiments; 50 cells were assessed per independent experiment.) Data represent mean \pm s.d. *P<0.05 (two-tailed t-test). (e) GFP-LC3-expressing NRK cells were transfected with nonspecific- (NS) or *Capzb*-RNAi. Cells were starved for 4 hours and stained with antibody to GFP. Cells were quantified for total

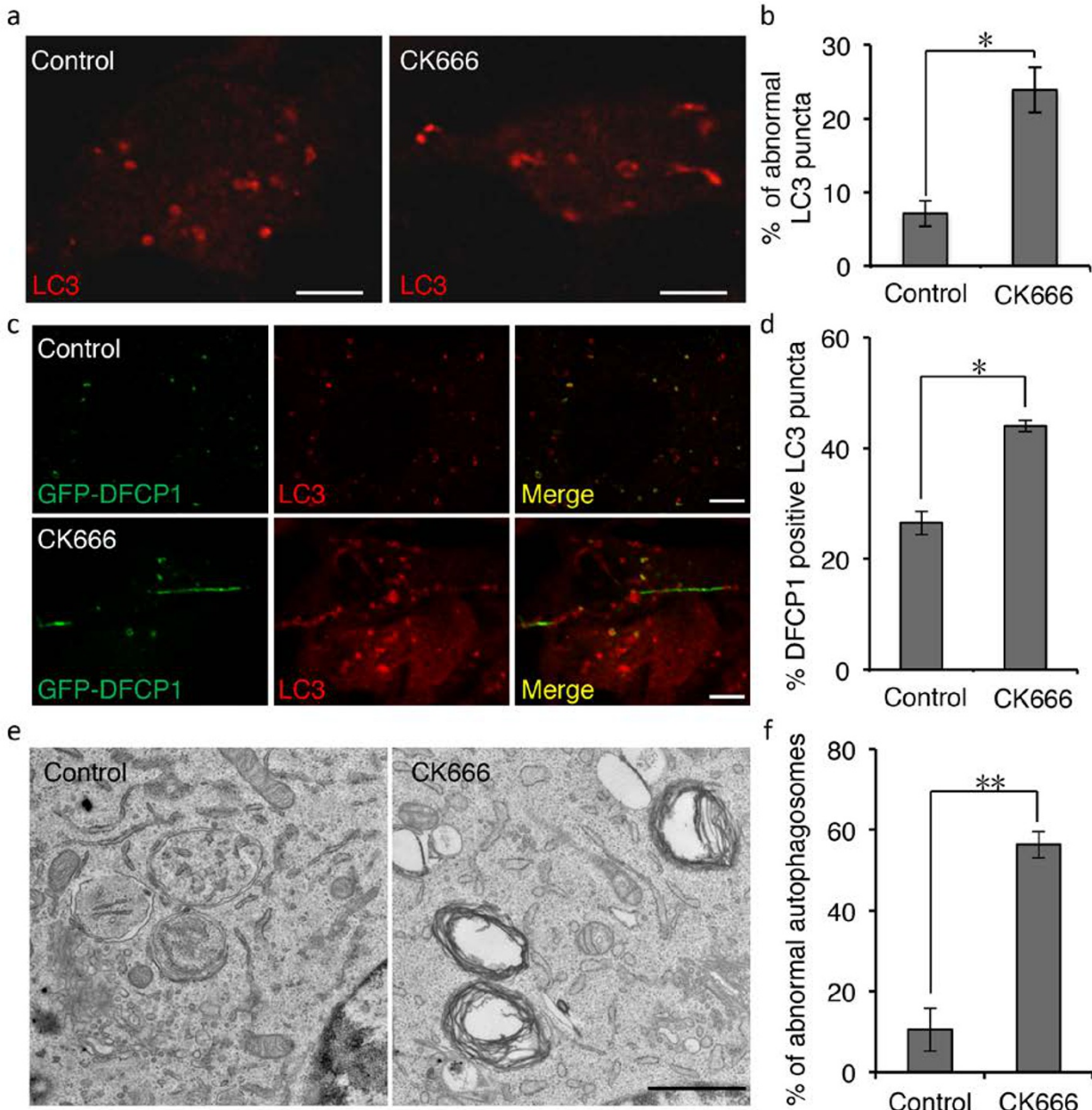
LC3 puncta. (n=3 independent experiments; 50 cells were assessed per independent experiment). Data represents mean \pm s.d. NS, no significant (two-tailed t-test). (f) Raw cells were transfected with nonspecific- (NS) or *Capzb*-RNAi. Cells were starved for 4 hours and stained with antibody to LC3. Scale bar, 5 μ m. (g) Cells from (f) were assessed for abnormal tubular LC3 puncta in a blinded fashion and quantified. (n=3 independent experiments; 100 cells were assessed per independent experiment.) Data represent mean \pm s.d. ***P<0.001 (two-tailed t-test). (h) Stable *Capzb* knockdown NRK cells were transfected with CapZ β -Myc. Cells were starved for 0 or 4 hours and stained with antibody to LC3. Scale bar, 5 μ m. (i) The expression level of CapZ β -Myc was verified by western blot. Uncropped images of blots are shown in Supplementary Fig. 9. (j) Cells from (h) were assessed for abnormal tubular LC3 puncta in a blinded fashion and quantified. (n=3 independent experiments; 100 cells were assessed per independent experiment.) Data represent mean \pm s.d. *P<0.05 (two-tailed t-test).

SUPPLEMENTARY INFORMATION



Supplementary Figure 3 CapZ regulates autophagy. (a) GFP-DFCP1-expressing NRK cells were transfected with nonspecific- (NS) or *Capzb*-RNAi. Cells were starved for 4 hours and stained with antibodies to GFP. Regions outlined with white dashed lines are magnified. Scale bars in full

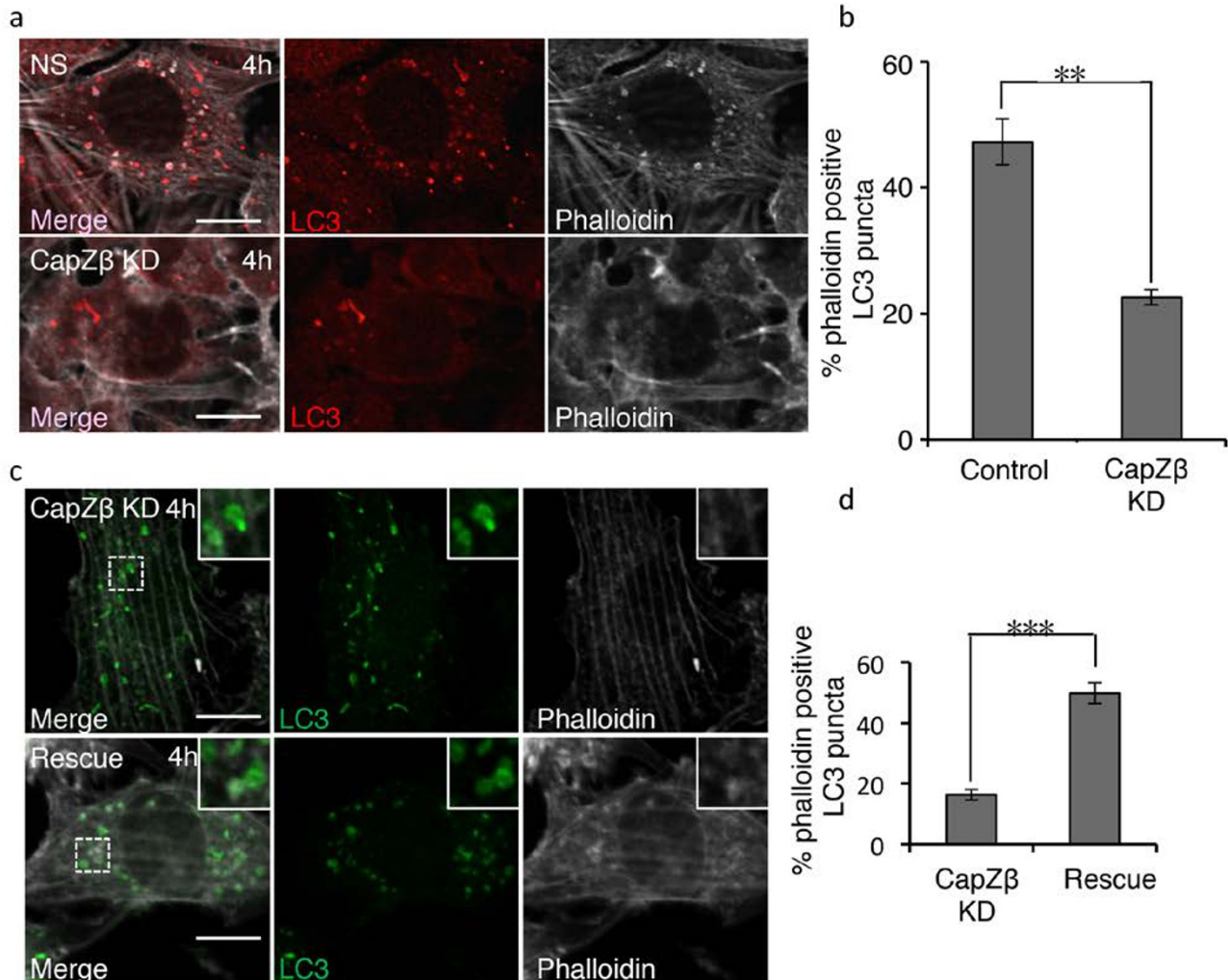
panels and zoomed panels correspond to 5 μ m and 2 μ m, respectively. (b) GFP-DFCP1-expressing NRK cells were transfected with nonspecific- (NS) or *Capzb*-RNAi. Cells were stained with antibodies to GFP and LC3. Scale bar, 5 μ m.



Supplementary Figure 4 Formation of abnormal LC3 puncta in CK666-treated cells. (a) NRK cells were starved for 2 hours, then 100 μ M CK666 was added to the starvation medium for 1 hour. Cells were stained with antibody to LC3. Scale bar, 5 μ m. (b) Cells from (a) were assessed for abnormal tubular LC3 puncta in a blinded fashion and quantified. (n=3 independent experiments; 100 cells were assessed per independent experiment.) Data represent mean \pm s.d. *P<0.05 (two-tailed t-test). (c) GFP-DFCP1-expressing NRK cells were starved for 2 hours, then 100 μ M CK666 was added to the starvation medium for 1 hour. Cells were observed by TEM. Scale bar, 1 μ m. (f) Cells from (e) were assessed for abnormal autophagosomes in a blinded fashion and quantified. (n=3 independent experiments; 60 cells were assessed per independent experiment.) Data represent mean \pm s.d. **P<0.01 (two-tailed t-test).

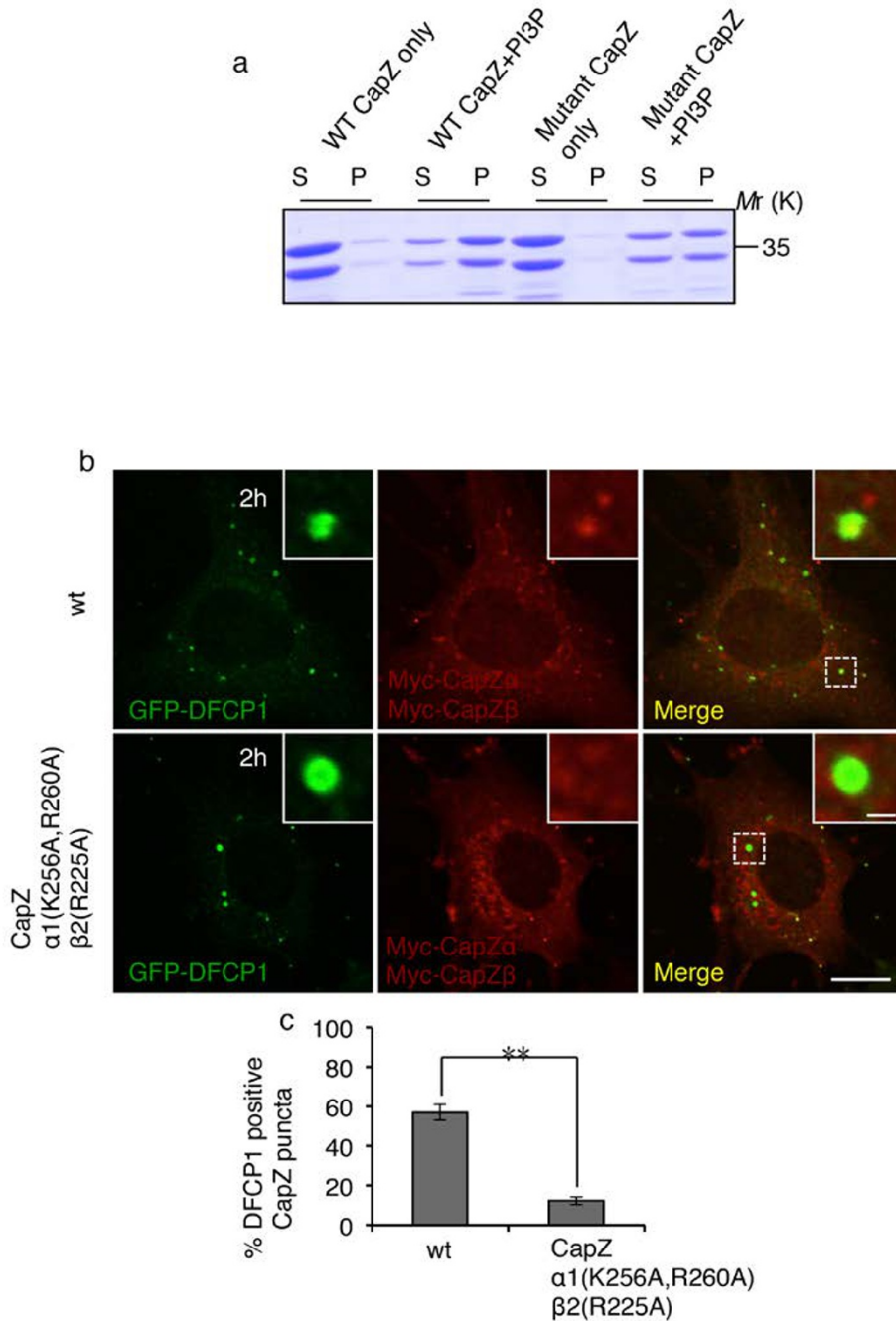
Scale bar, 5 μ m. (d) Cells from (c) were assessed for DFCP1/LC3 double-positive puncta in a blinded fashion and quantified. (n=3 independent experiments; 50 cells were assessed per independent experiment.) Data represent mean \pm s.d. *P<0.05 (two-tailed t-test). (e) NRK cells were starved for 2 hours, then 100 μ M CK666 was added to the starvation medium for 1 hour. Cells were observed by TEM. Scale bar, 1 μ m. (f) Cells from (e) were assessed for abnormal autophagosomes in a blinded fashion and quantified. (n=3 independent experiments; 60 cells were assessed per independent experiment.) Data represent mean \pm s.d. **P<0.01 (two-tailed t-test).

SUPPLEMENTARY INFORMATION



Supplementary Figure 5 CapZ regulates actin puncta formation. (a) NRK cells were transfected with nonspecific- (NS) or *Capzb*-RNAi. Cells were starved for 0 or 4 hours and stained with phalloidin and antibody to LC3. Scale bar, 5 μ m. (b) Cells from (a) were quantified for phalloidin-positive LC3 puncta. (n=3 independent experiments; 50 cells were assessed per independent experiment.) Data represent mean \pm s.d. **P<0.01 (two-tailed t-test). (c) Stable *Capzb* knockdown NRK cells were transfected with

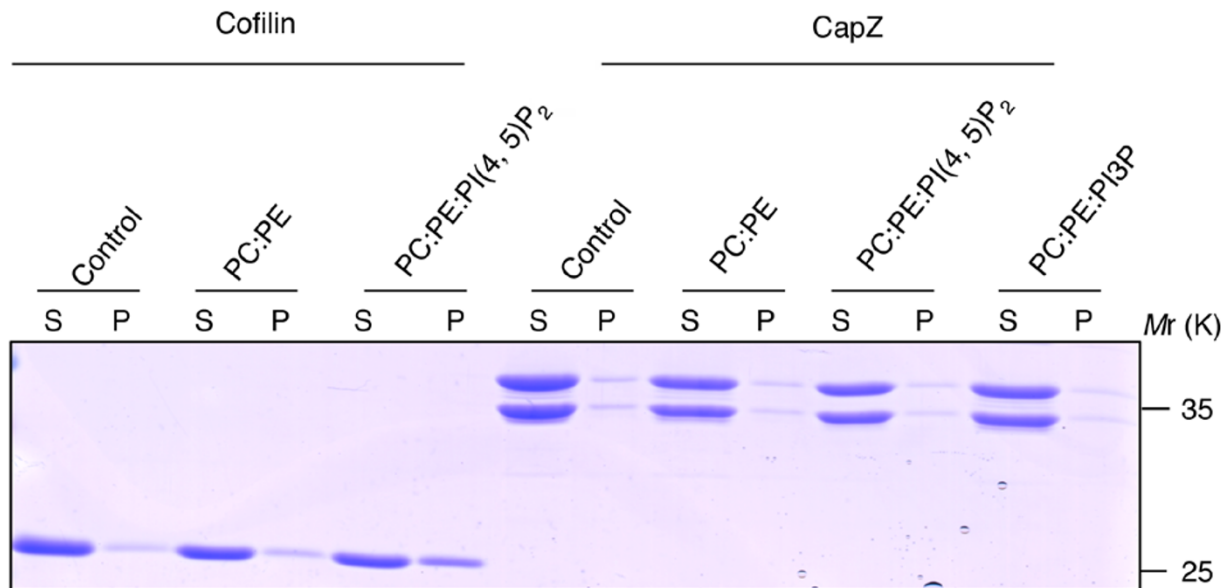
CapZ β -Myc, then starved for 0 or 4 hours and stained with antibody to LC3 and phalloidin. Regions outlined with white dashed lines are magnified. Scale bars in full panels and zoomed panels correspond to 5 μ m and 1 μ m, respectively. (d) Cells from (c) were quantified for phalloidin-positive LC3 puncta. (n=3 independent experiments; 100 cells were assessed per independent experiment). Data represent mean \pm s.d. ***P<0.001 (two-tailed t-test).



Supplementary Figure 6 (a) CapZ mutant has impaired binding activity to PI3P. Co-sedimentation assay with PI3P micelles and recombinant WT CapZ α CapZ β and CapZ α (K256A, R260A)CapZ β (R225A). Proteins in supernatant (S) and precipitate (P) were visualized by SDS-polyacrylamide gel electrophoresis and stained with Coomassie brilliant blue. The experiment was repeated 3 times. Uncropped images of gels are shown in Supplementary Fig. 9. (b) GFP-DFCP1-expressing NRK cells were transfected with wild type

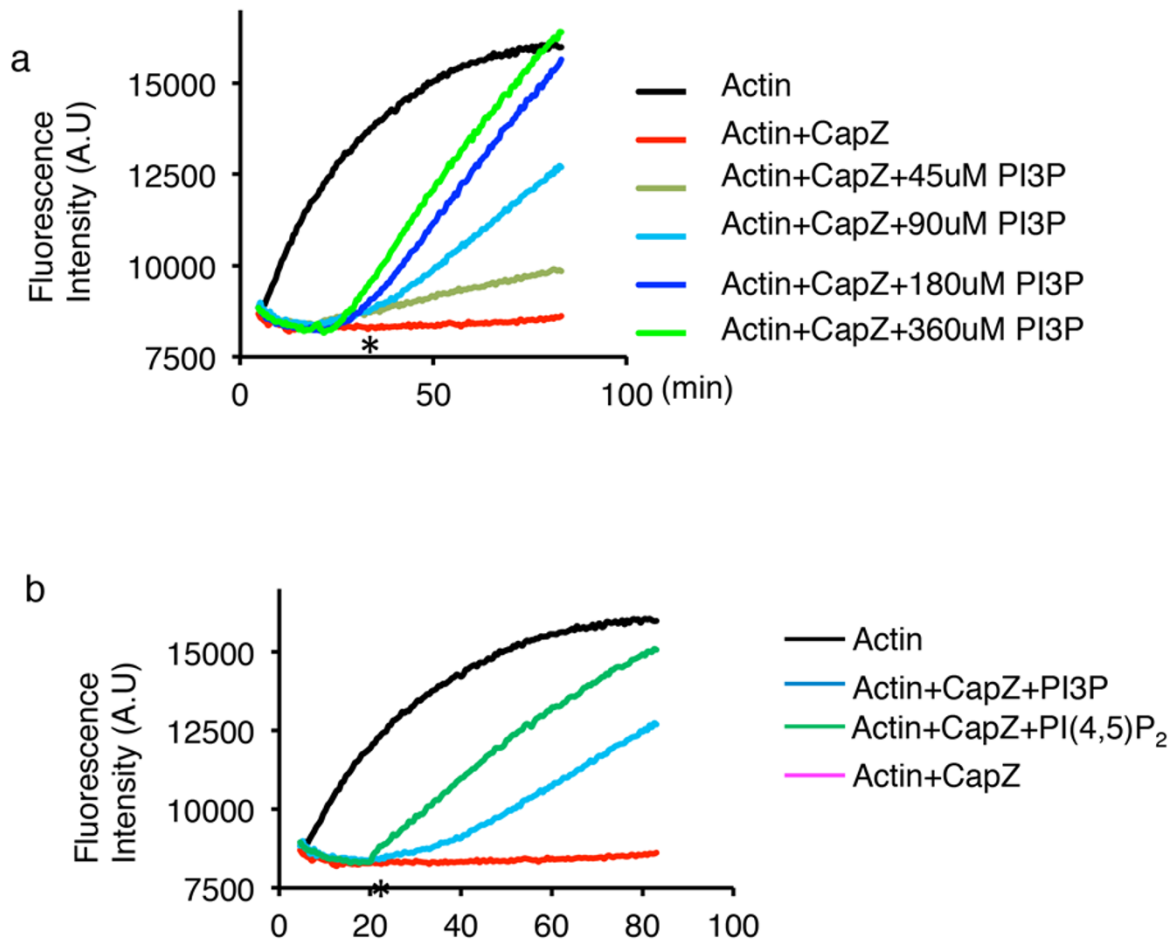
or mutant CapZ α (K256A, R260A)-Myc and CapZ β (R225A)-Myc. Cells were then starved for 2 hours and stained with antibodies to GFP and Myc. Regions outlined with white dashed lines are magnified. Scale bars in full panels and zoomed panels correspond to 5 μ m and 1 μ m, respectively. (c) Cells from (b) were quantified for CapZ-positive DFCP1 puncta. (n=3 independent experiments; 50 cells were assessed per independent experiment.) Data represent mean \pm s.d. **P<0.01 (two-tailed t-test).

SUPPLEMENTARY INFORMATION



Supplementary Figure 7 Co-sedimentation assay of CapZ α CapZ β /Cofilin with liposomes containing 20% PI3P or PI(4,5)P₂. Proteins in supernatant (S) and precipitate (P) were visualized by SDS-polyacrylamide

gel electrophoresis and stained with Coomassie brilliant blue. The experiment was repeated 3 times. Uncropped images of gels are shown in Supplementary Fig. 9.



Supplementary Figure 8 (a) Uncapping efficiency of PI3P is dose-dependent. Uncapping assays were performed with 2 μ M α -actin and 10 nM CapZ. The indicated concentrations of PI3P were added to the reactions 20 min after the start point. Uncapping efficiency was measured by the increase in the rate of actin polymerization. (b) Comparison of the effects of

PI(4,5)P₂ and PI3P on uncapping of actin filaments. Uncapping assays were performed with 2 μ M α -actin and 10 nM CapZ. 90 μ M PI3P (cyan curve) or PI(4,5)P₂ (blue curve) was added to the reactions. Both PI3P and PI(4,5)P₂ induced a large increase in the rate of actin polymerization from capped actin filaments.

SUPPLEMENTARY INFORMATION

Fig. 5c

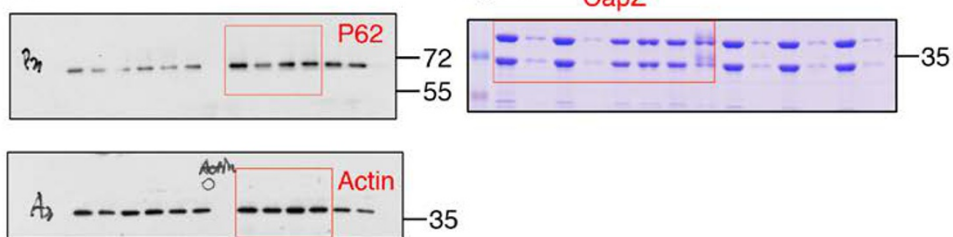
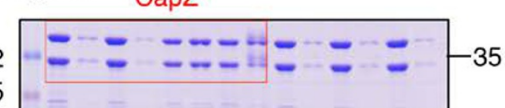
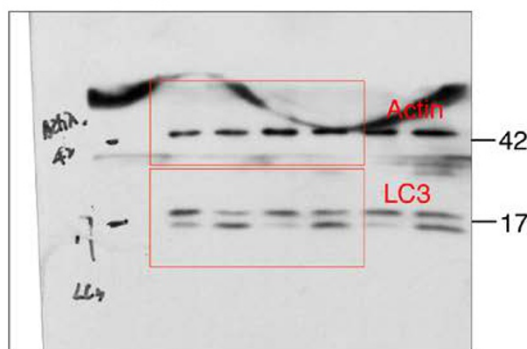


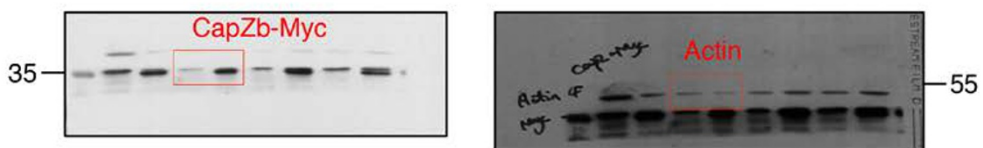
Fig. 7d CapZ



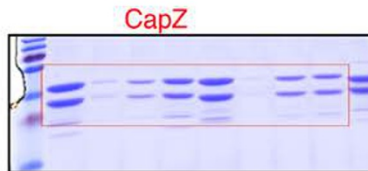
Supplementary Fig. 4b



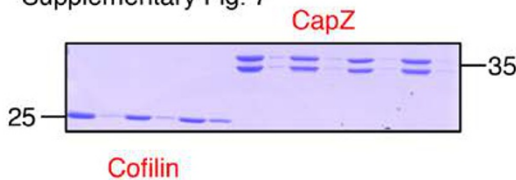
Supplementary Fig. 5f



Supplementary Fig. 6a



Supplementary Fig. 7



Supplementary Figure 9 Scans of original Western Blot analyses and SDS-PAGE followed by Coomassie brilliant blue analysis. Cropped regions are indicated by the red boxes. Molecular weights are reported.

SUPPLEMENTARY INFORMATION

Supplementary video 1 The kinetic of serum/glutamine starvation induced autophagy. GFP-LC3-expressing NRK cells were starved for 4 hours in serum/glutamine starvation medium. Cells were observed by spinning disc microscope. Time interval, 10 minutes.